

ABSTRACT

HEGDE, AMRUTHKIRAN. Experimental Investigation into Shock Induced Corner Boundary Layer Separation. (Under the direction of Dr.Venkateswaran Narayanaswamy).

This work is motivated to enhance our current understanding of shock-induced separation of junction/corner boundary layer, which has common occurrence in supersonic inlets and wing-body junctions. Experiments are conducted to investigate the interaction between an oblique shock wave and a corner boundary layer (called corner-SBLI) in our supersonic wind tunnel facility. Wall pressure measurements are taken in the regions of corner flow separation and the upstream boundary layer to unravel the dynamic interactions between the upstream boundary layer and different locations inside corner-SBLI. Additionally, flow visualization is obtained, which helps in qualitative understanding of the separated corner flow. The experiments are performed over different shock strengths and Mach numbers to obtain a detailed understanding of the evolution of the corner-SBLI dynamics with increasing separation strength and compressibility.

© Copyright 2015 Amruthkiran Hegde

All Rights Reserved

Experimental Investigation into Shock Induced Corner Boundary Layer Separation

by
Amruthkiran Hegde

A thesis submitted to the Graduate Faculty of
North Carolina State University
in partial fulfillment of the
requirements for the degree of
Master of Science

Aerospace Engineering

Raleigh, North Carolina

2015

APPROVED BY:

Dr.Hong Luo
Committee Member

Dr.Hassan Hassan
Committee Member

Dr.Venkateswaran Narayanaswamy
Committee Chair

ACKNOWLEDGMENTS

I would like to thank Dr. Venkateswaran Narayanaswamy, who, as my graduate advisor helped me understand the area of Shock Wave Boundary Layer Interaction. His encouragement to try different things helped me to bring out my imagination and apply it to research. His guidance has truly helped me grow into an Aerospace Engineer. I would like to extend my gratitude to Mr. Steve Cameron, the specialty trades technician at NC State University, who was kind enough to spend time with me and explain the nuances of machining without which my research would not have been possible. I would like to thank my father who helped me realize my graduate education and my mother, who has been the strength throughout my life. I thank all my friends who have been my emotional support throughout my education.

TABLE OF CONTENTS

LIST OF TABLES.....	v
LIST OF FIGURES	vi
CHAPTER-1. INTRODUCTION TO SHOCK WAVE/TURBULENT BOUNDARY LAYER INTERACTION.....	1
CHAPTER-2. A REVIEW OF PAST RESEARCH AND MECHANISM OF SBLI.....	4
2.1. Centerline Flow.....	4
2.2 Corner Flow.....	8
CHAPTER-3. RESEARCH MOTIVATION.....	12
CHAPTER-4. EXPERIMENTAL FACILITY DESIGN AND ASSISTING SET UPS.....	13
4.1 Wind Tunnel Design.....	13
4.2 Schlieren Imaging.....	13
4.3 Surface Flow Visualization.....	15
4.4 Unsteady Pressure Measurements.....	15
4.5 Auxiliary Experimental Set up.....	16
CHAPTER-5. FLAT PLATE BOUNDARY LAYER MEASUREMENT	18
5.1 Experimental Setup.....	18
5.2 Experimental procedure	20
5.3 Results and Discussion	24
CHAPTER-6. SBLI IN EXPERIMENTAL SET-UP.....	24
6.1 Incident shock reflection method.....	25
6.1.1. Experimental Setup.....	25
6.1.2. Surface Flow Visualization.....	26
6.1.3. Schlieren Imaging	27
6.2 Flow Separation by compression ramp.....	28
6.2.1 Experimental setup.....	28
6.2.2. Baseline Flow.....	29
6.2.3. Results and Discussion-Shock Induced separation with 12° and 16° compression ramp.....	32
6.2.3.1 Surface Flow Visualization with 12° ramp (Mach 2.5).....	32

6.2.3.2 Surface Flow Visualization with 12° ramp (Mach 3.3).....	36
6.2.3.3 Surface Flow Visualization with 16° ramp (Mach 2.5).....	37
6.2.3.4 Surface Flow Visualization with 16° ramp (Mach 3.3).....	41
6.2.4 Static Pressure Measurements.....	43
CHAPTER-7. SUMMARY AND FUTURE WORK.....	57
REFERENCES.....	59
APPENDIX.....	61

LIST OF TABLES

Table 1. Table of Incoming Boundary Layer Data.....	23
---	----

LIST OF FIGURES

Figure 1. Image of Rectangular to Elliptic Shape Transition Inlet (REST).....	2
Figure 2. Schematic of wave pattern in a compression corner (from Vishwanath 1988).....	5
Figure 3. Schematic of wave pattern without separation (a) compression corner (b) incident shock (from Vishwanath 1988).....	5
Figure 4. The three canonical geometries depicting SBLI (a) compression corner (b) incident shock (c) blunt fin (from Clemens et al. 2013).....	7
Figure 5. Proposed three-dimensional shock structure due to corner induced bifurcation (from Burton et al. 2010).....	11
Figure 6. Schlieren Setup.....	14
Figure 7. Positioning and numbering of the pressure transducers.....	16
Figure 8. Schematic of the auxiliary set up.....	17
Figure 9. Schematic of flat plate set up.....	19
Figure 10. A view of the flat plate set up in the wind tunnel.....	20
Figure 11. (a) boundary layer profile at Mach 2.5 (b) pitot pressure profile at Mach 2.5 (b) u^+ Vs y^+ at Mach 2.5.....	22
Figure 12. (a) boundary layer profile at Mach 3.3 (b) pitot pressure profile at Mach 3.3 (b) u^+ Vs $\ln y^+$ at Mach 3.3.....	23
Figure 13. Schematic of corner flow.....	26
Figure 14. Flow Visualization by incident shock method.....	27
Figure 15. Flat plate, fence and ramp set up showing SBLI and corner flow.....	29

Figure 16. (a) flow at Mach 2.5 (b) flow at Mach 3.3.....	30
Figure 17. Surface Flow Visualization with 12° ramp (Mach 2.5) (a) side view (b) isometric view(c) top view.....	33
Figure 18. Top view of Surface Flow Visualization with 12° ramp (Mach 3.3).....	36
Figure 19. Surface Flow Visualization with 16° ramp (Mach 2.5) (a) top view (b) isometric view (c) side view.....	38
Figure 20. Top view of Surface Flow Visualization with 16° ramp (Mach 3.3).....	41
Figure 21. (a) Avg. Prms/Pwall for Centerline flow at Mach 2.5 (b) Avg. Prms/Pwall for Centerline flow at Mach 3.3 (c) Avg. Prms/Pwall for Corner flow at Mach 2.5 (d)Avg. Prms/Pwall for Corner flow at Mach 3.3.....	44
Figure 22. (a) Avg. Pwall/Pinf for Centerline flow at Mach 2.5 (b) Avg. Pwall/Pinf for Centerline flow at Mach 3.3 (c) Avg. Pwall/Pinf for Corner flow at Mach 2.5 (d)Avg. Pwall/Pinf for Corner flow at Mach 3.3.....	46
Figure 23. Power Spectral Density for 12° ramp (Centerline flow) at Mach 2.5.....	48
Figure 24. Power Spectral Density for 12° ramp (Centerline flow) at Mach 3.3.....	49
Figure 25. Power Spectral Density for 16° ramp (Centerline flow) at Mach 2.5.....	50
Figure 26. Power Spectral Density for 16° ramp (Centerline flow) at Mach 3.3.....	51
Figure 27. Power Spectral Density for 12° ramp (Corner flow) at Mach 2.5.....	52
Figure 28. Power Spectral Density for 12° ramp (Corner flow) at Mach 3.3.....	53
Figure 29. Power Spectral Density for 16° ramp (Corner flow) at Mach 2.5.....	54
Figure 30. Power Spectral Density for 16° ramp (Corner flow) at Mach 3.3.....	55

CHAPTER-1. INTRODUCTION TO SHOCK WAVE/TURBULENT BOUNDARY LAYER INTERACTION

Shock Wave/Turbulent Boundary Layer Interaction (SBLI) is a common feature and a complex flow phenomena in supersonic jet engine inlets, reaction jets, wings on transonic aircrafts and in experimental facilities such as supersonic wind tunnels.

In high-speed air-breathing vehicles, the air must be brought to subsonic speeds at the engine inlets from the supersonic inflow Mach number. In the mixed compression inlet intakes this is achieved through a series of oblique shock waves with a terminal normal shock wave. This helps in better pressure recovery and avoids stagnation losses. In this process, the shock wave, acts as an adverse pressure gradient and interacts with the turbulent boundary layer that develops on the rectangular inlet channel walls. Strong interactions cause boundary layer thickening and can trigger flow separation. Flow separation occurs when the fluid momentum is not enough to overcome the adverse pressure gradient imposed by the impinging shock wave. This leads to temporal and spatial distortion of the overall flow field and reduces the effective cross sectional of fluid flow causing choking and engine unstart. Unstart occurs when the fluid momentum upstream is greater than the fluid downstream resulting in the shock system moving upstream and finally out of the inlet. The unsteadiness of the interaction further causes aircraft buffeting, inlet instability in supersonic vehicles and an additional problem of severe thermal loading in hypersonic vehicles. Also, the coupling of pressure oscillations with the resonant frequency of the aircraft structures leads to high amount of aerostructure fatigue, which ultimately may result in the catastrophic failure of the aircraft.

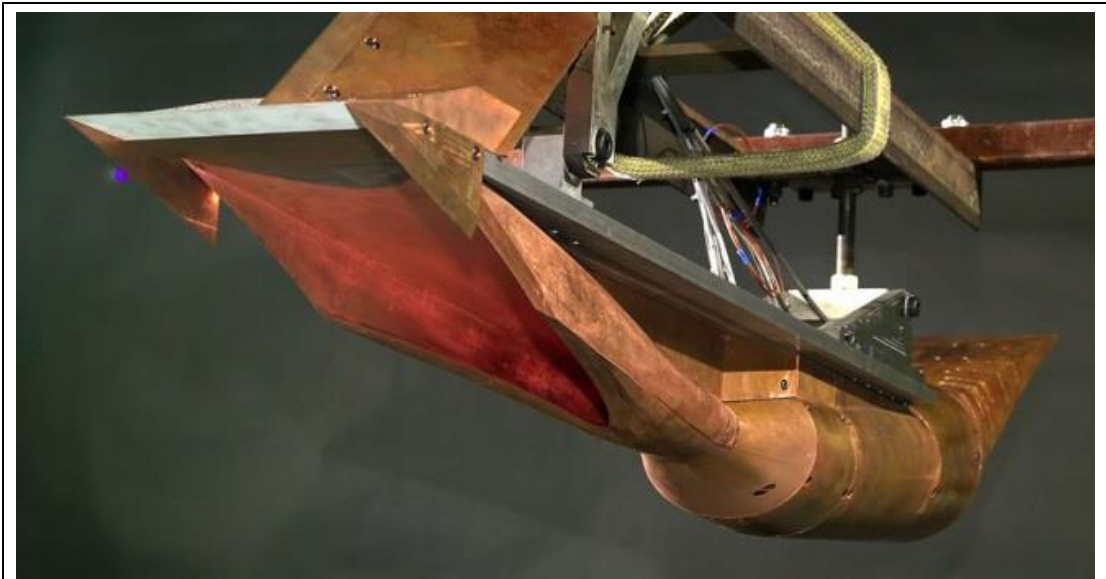


Figure 1. Image of Rectangular to Elliptic Shape Transition Inlet (REST)

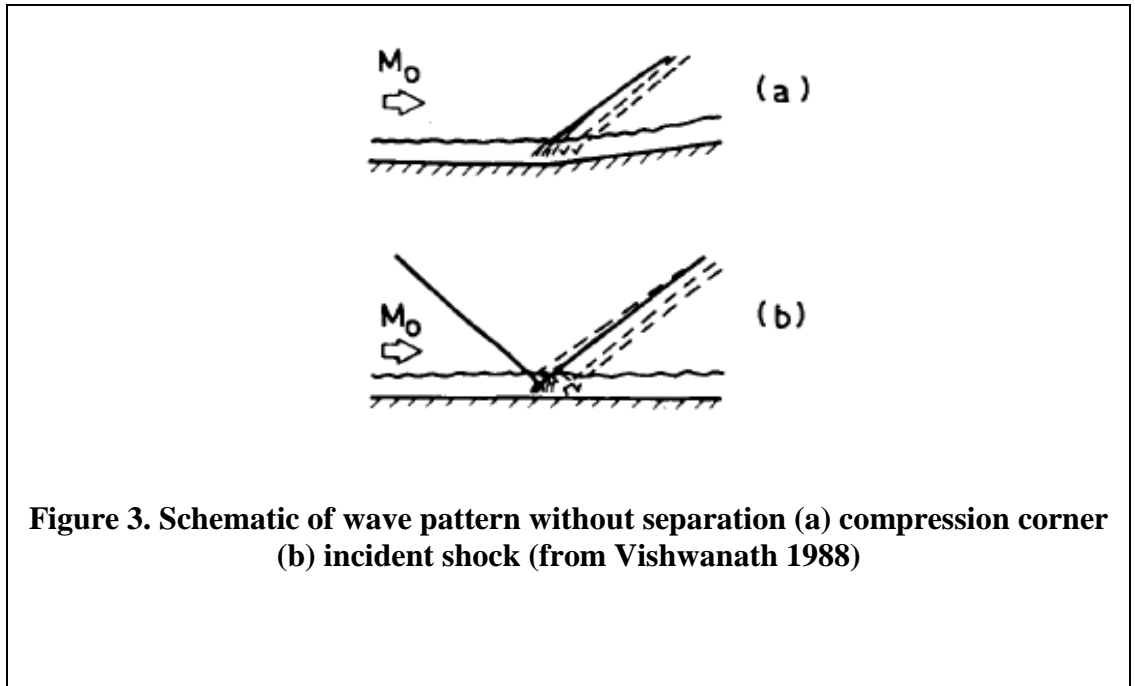
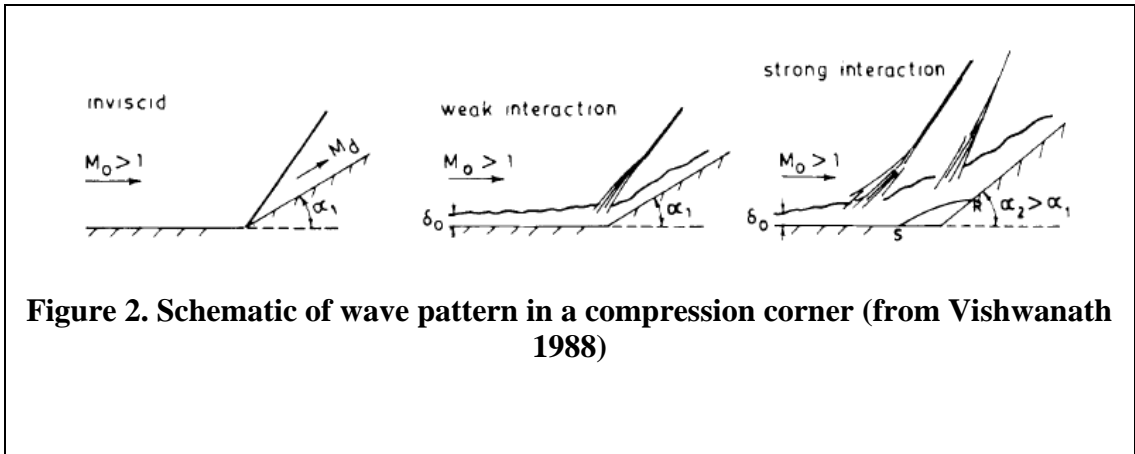
A large portion of research on SBLI till date has mainly focused only on the centreline flow in SBLIs, away from the corners, without taking the corner effect into consideration and has treated the interaction as a two dimensional interaction. However, streamwise corner flow that forms at the intersection of the walls which enclose the channels is an unavoidable feature in the supersonic jet inlet and experimental facilities. This corner flow which encompasses the boundary layer of both the walls imparts three dimensionality into SBLIs (meaning all the three components of velocity having mean and fluctuations) and hence the SBLIs can seldom be practically treated as 2-D. For e.g., as seen in figure.1, in the REST inlet design in most scramjet vehicles, we observe a change of cross section from rectangular at the inlet to elliptical at the combustion chamber. In such a case, the boundary layers that develop on the walls are

highly three dimensional. Through recent research it has been shown that the corner effects in SBLI are even felt on the flow centreline, as observed in different shock induced separation behavior at different experimental facilities for experiments with comparable Reynolds Number emphasizing the fact that they can no longer be ignored. The lack of understanding of the physics behind corner flows, even today, thus represents a major hurdle in modeling the SBLI through numerical methods such as Reynolds Averaged Navier Stokes(RANS), Large Eddy Simulations(LES) and detached eddy simulation (DES) codes that are capable of capturing the flow structure in three dimensional geometries with corners where shock waves are present. Hence the research in the direction of corner flows and their effects on the overall flowfield has gained motivation over time with researchers proposing several mechanisms over the years through which the corner flow affects the overall flow field.

CHAPTER-2. A REVIEW OF PAST RESEARCH AND MECHANISM OF SBLI

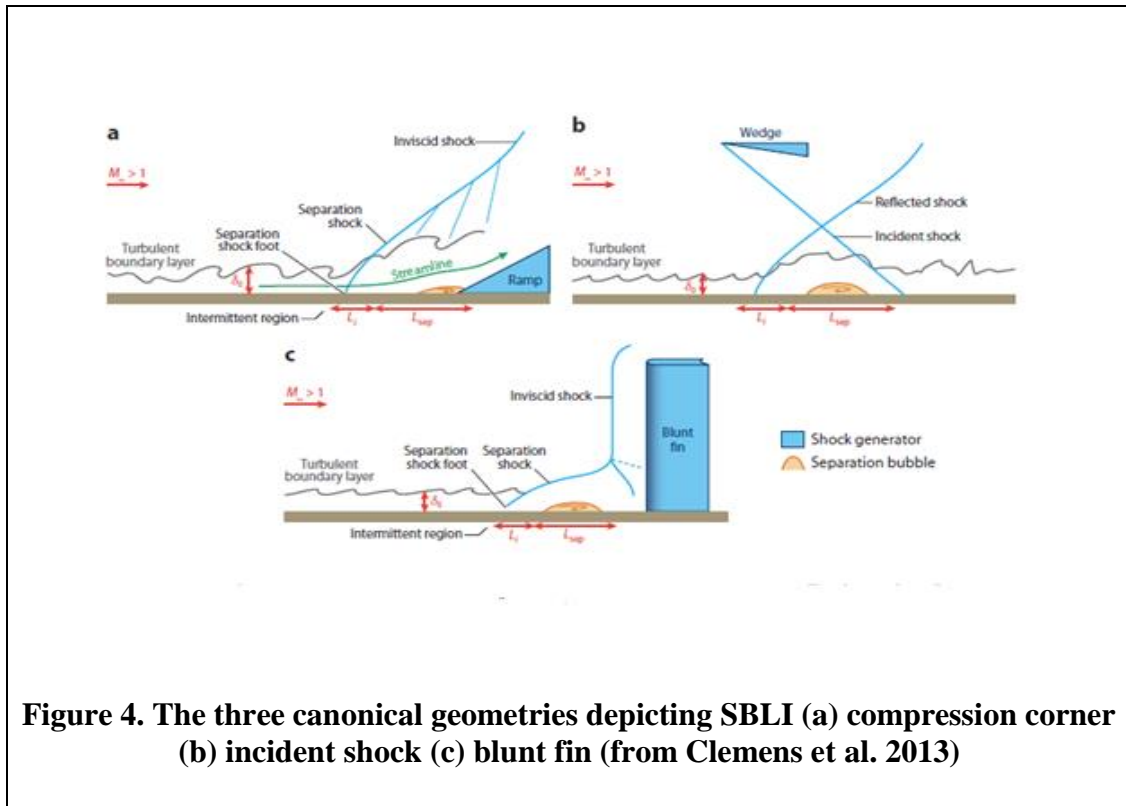
2.1. Centerline Flow

When a shockwave meets a surface in inviscid flow, it causes an abrupt pressure rise across the surface. However, due to the viscous nature of fluids, a boundary layer always develops near the surface when a fluid flows over a body. Further, in supersonic flow, there is always a region in the boundary layer below which the flow is subsonic. This subsonic flow cannot support an abrupt pressure rise as that caused by the shock wave. Thus the shock wave terminates at the sonic line in the boundary layer (this is called the shock foot) and imparts pressure disturbances which travel both upstream and downstream of the flow. The subsonic stream tubes thicken in reaction to the adverse pressure gradient and generate compression waves which travel in the supersonic part of the boundary layer. These waves cause additional pressure rise and readjustment of the subsonic part of the boundary layer. This cycle continues until there is a compatibility between the gradual pressure rise in the subsonic region of the boundary layer with the abrupt pressure rise in the outer inviscid flow. If the pressure rise is “weak”, then the boundary layer can negotiate the pressure rise without separation. In the case of a reflected shock wave, for interaction without separation a secondary set of waves are formed due to the refraction of the incident shock wave. In the case of a compression corner, the secondary waves are formed partly due to the streamline curvature of the stream tubes and partly due to the compression waves which generate waves that get reflected at the sonic line of the boundary layer. The strong and weak interaction and interaction without separation are depicted in figure 2 and figure 3 respectively.



As pressure rise builds with increasing shock strength, the fluid in the boundary layer does not have enough momentum to overcome the adverse pressure gradient imposed by the outer inviscid flow and starts decelerating past the shock wave. The boundary layer eventually separates with the fluid reversing its flow direction. This is the point of incipient flow separation. It is marked with the appearance of separation bubble. The upstream separated boundary layer lifts over the bubble. In the case of a ramp, this deflection leads to the formation of a separation shock. With further increase in the inviscid disturbance, the separation bubble grows in size pushing the separation/reflected shock further upstream. The separation bubble grows as a free shear and acquires kinetic energy as a result of mixing. Once it acquires enough energy, it overcomes the adverse pressure gradient leading to flow reattachment. The lengthscale, L_{sep} between the flow separation and reattachment is called the length of separation. This lengthscale keeps varying, as one of the most striking features of the separation bubble is its unsteady breathing motion with fluid entering and emptying it cyclically. The parameters governing this feature is under debate with researchers arguing that both upstream and downstream flow conditions contribute towards its growth and collapse. Also, separation/reflected shock foot oscillates back and forth over a region of L_i called the intermittent region. Thus the motion of the separation bubble and the oscillations of the shock foot collectively represent the flow unsteadiness. Unsteady pressure measurements taken under the regions of incoming boundary layer, intermittent region and the separation bubble and plotting the corresponding pressure density spectra has shown that the intermittent region is characterized by low frequency oscillations that dominate the spectra while the incoming turbulent boundary layer and the separation bubble exhibit high frequency oscillations. Further,

with increase in Mach number, the shock sweeps larger lengths with lower frequencies due to which the SBLI along the centerline are generally characterized as interactions with low frequency unsteadiness. Figure. 4 shows the schematics of the canonical geometries and the different regions in SBLI.



A bulk of the knowledge on the characteristics of SBLI is from the research that has mainly concentrated on a normal shock turbulent boundary layer interaction, with the parameters governing the condition of flow separation in a normal SBLI being the focus of research over

the time. Principal contributors in this area over the last sixty years include Ackeret, Feldmann & Rott (1947), Seddon (1960), Kooi (1978), Delery (1985) and Sajben et al. (1991). Researchers agree that interaction strength (incoming flow Mach number) is the single most important factor in determining whether a turbulent boundary layer separates or remains attached through a normal SBLI. Factors such as the incompressible boundary layer shape factor ahead of the interaction (H_{i0}) with the Reynolds number (Re) effect incorporated into it. Bruce et al. (2011) summarized the experiments on SBLIs conducted at different facilities till then. Combining the results from the experiments done previously, they came up with a parameter which is an aspect ratio, δ^*/w (δ^* is the boundary layer displacement thickness and w is the width of the channel) and plotted it against the Mach number thus predicting the separation of flow. The results from the previous experiments collapsed into a much clearer trend along this plot. This parameter also indicates the three-dimensionality of a particular flow. Values of δ^*/w close to zero correspond to experiments that are nominally two dimensional such as axisymmetric facilities or those in large facilities with thin boundary layers, while large values of δ^*/w represent more highly confined experiments in small facilities with relatively thick boundary layers.

2.2 Corner Flow

Experiments done by Chriss et al.(1989) and Titchener & Babinsky (2011) have shown that flows along corners have effects far away from it, even along the flow centreline. Burton & Babinsky (2012), Bruce, Burton, Titchener & Babinsky (2011) and Burton, Babinsky & Bruce (2010), have contributed significantly towards our knowledge of corner effects through their recent work on normal SBLI in rectangular channels at low Mach numbers of 1.4-1.5. The

corner SBLI was manipulated by corner suction and vortex generators to examine the coupling between corner separation and separation away from the corner. A reduction in the spanwise corner separation marked by a centerline separation was observed due to flow suction through slots positioned in the corners at locations upstream of the SBLI, while increased corner separation without any centreline flow separation was seen when corner vanes acting as vortex generators were positioned upstream of the flow. Experiments were carried out with each of the modifications separately and conclusions on the effects of corner flow were drawn after observing the flow visualizations and static wall pressure measurements, taken along flow centerline and at a few spanwise distance away from it.

Suction decreases the spanwise corner separation as it produces a slight drop in pressure ahead of the shock and a reduced upstream influence, which leads to a sharper pressure rise through the initial part of the SBLI. This is also seen from the comparison of pressure profiles of the centreline flow with and without suction, which indicate a sharper pressure near the regions of the shock, in the case of suction than the baseline flow. This increased pressure gradient is the likely cause of the centerline separation. There is a compression fan ahead of the shock in the baseline flow which is replaced by the λ -shock foot with a relatively weak rear leg which is an indication of a decreased interaction length that favours centreline separation. Also, there is a decrease in the pressure smearing near the tunnel corners as compared to the baseline flow, caused by a decrease in the upstream influence of SBLI. This smearing of pressure does not reach the entire span of the flow. Hence the flow between the corner and the centreline remains attached. The pressure profiles taken at the centre and at an off centre location present an interesting feature of the flow. The adverse pressure gradient is steeper for the baseline case

than the two test cases. This shows that the pressure gradient is smeared over a large region in the two test cases thus making the bifurcating shock foot 3-D.

The increase in corner separation due to vortices produced by the corner vanes decreases the adverse pressure gradients along the centre as seen in the pressure profiles, by modifying the bifurcated shock structure. The increase in the corner separation acts as a blockage thus reaccelerating the post shock flow, reducing the downstream pressure. These are the two reasons for the absence of centreline flow separation. Finally, the conclusions aid in differentiating the flow structure along the corner and centreline. While the separated centreline flow is relatively two-dimensional, with reversed flow, a separation bubble and well-defined points of separation and reattachment, the corner flow separation is highly three dimensional, with vortex formation and no well-defined points of reattachment and separation. This proposed mechanism of SBLI is depicted in figure 5.

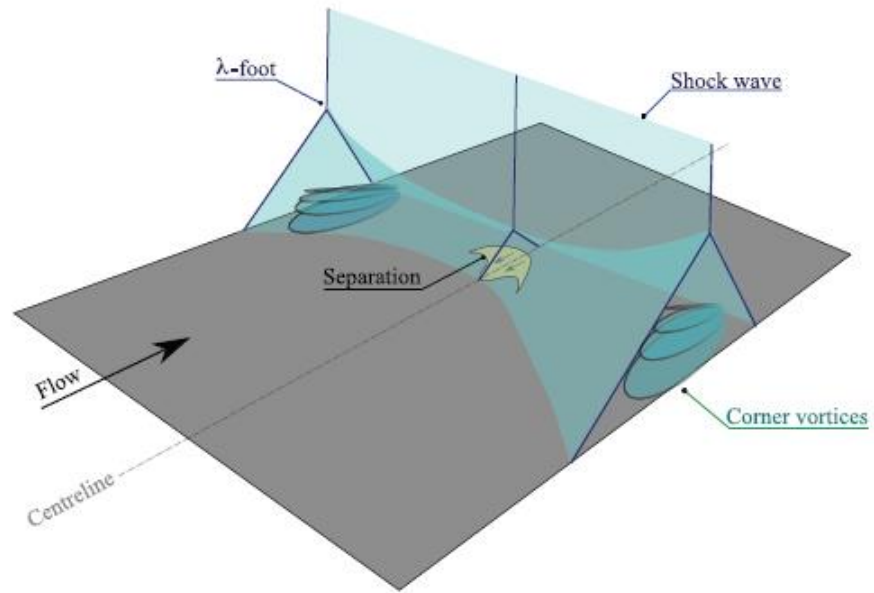


Figure 5. Proposed three-dimensional shock structure due to corner induced bifurcation (from Burton et al. 2010)

CHAPTER-3. RESEARCH MOTIVATION

As mentioned in the previous discussion, the past research on corner SBLI in experimental facilities was mainly carried out by generating a normal shock wave, since in practical conditions too, the series of oblique shocks generated at the face of the engine inlet ultimately terminate with a normal shock at the face of the engine. Hence the understanding of the flow properties in the vicinity of the normal shock would contribute towards improving the engine inlet designs. However, the oblique shock that is generated at the face of the inlet is the cause for the initial alteration of the incoming flow and there have been only a few instances where the flow separation produced by an oblique shock wave have been researched. Even in those cases, no attempts were made to obtain quantitative data at the corner. Hence, the questions on the mean flow structure of a separated corner flow, the wall-pressure fluctuations at different locations inside the corner flow in an oblique shock induced SBLI remain unanswered. This motivated the present work wherein, the oblique shock SBLI was simulated by allowing a pair of corner boundary layers to grow at the intersections of a flat plate and two perpendicular fences and separating this flow with an oblique shock wave generated with a compression ramp installed downstream in between the fences. Wall static pressure measurements taken along the centre and corner helped in gaining an insight into the pressure trend in the region of SBLI. Additionally, qualitative analysis of the flow was done through flow visualization which helped in identifying the different features in the region of flow separation and thereby establish a picture of the re adjusted shock structure.

CHAPTER-4. EXPERIMENTAL FACILITY DESIGN AND ASSISTING SET UPS

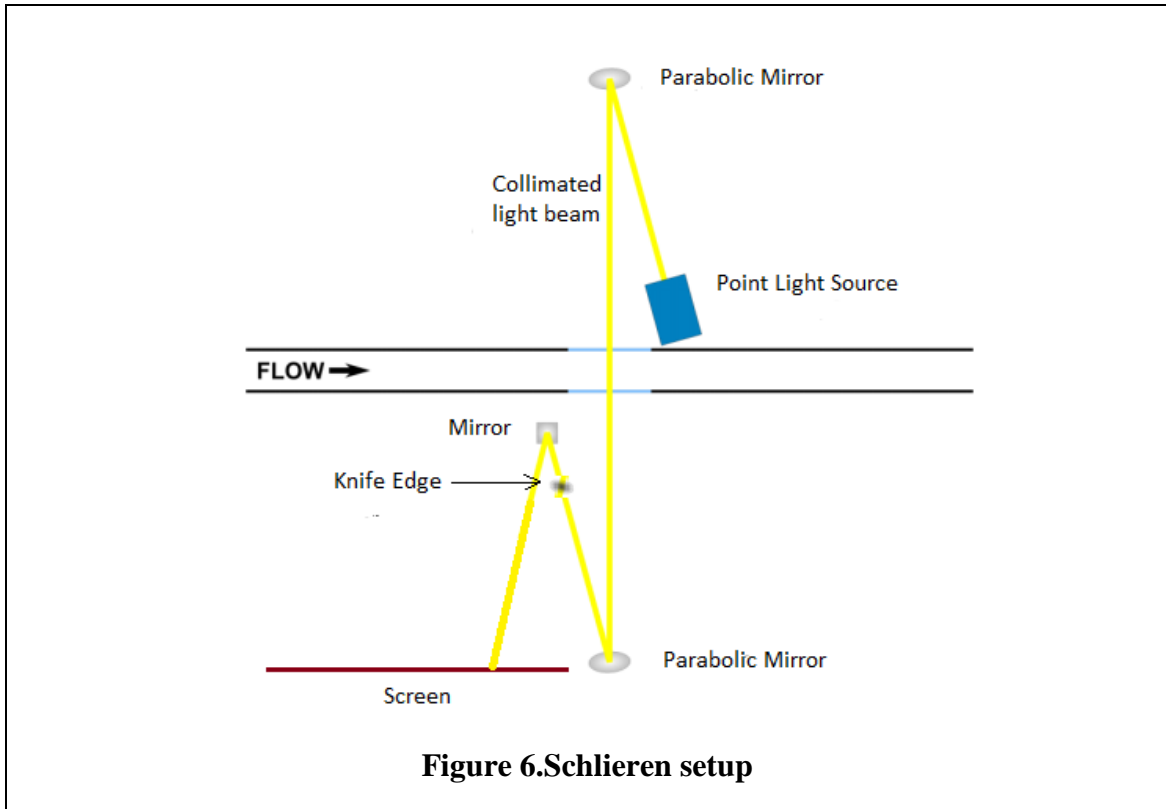
4.1 Wind Tunnel Design

The experimental investigation was undertaken at the Turbulent Shear Flow Laboratory at the North Carolina State University. This facility is a blow down type variable Mach number wind tunnel with a Mach number range of 1.5-4, from Aerolab LLC., that exhausts into ambient air. The test section has a square cross section area of 152.4 mm length and 152.4 mm width and is preceded by a convergent-divergent nozzle and a stagnation chamber. It can be viewed on either sides by windows made of optical grade fused silica which has an approx. cross section area of 454.02 mm length, 152.78 mm width and is 31.75 mm thick. The aluminum frame of the windows has six clearance holes for screws, that are drilled at its base, along its length and are 76.2 mm apart from each other. This is to facilitate set ups that span the width of the wind tunnel and need to be installed on its floor. The wind tunnel was operated through a LabVIEW VI set up on a PC.

4.2 Schlieren Imaging

Schlieren Imaging is a nonintrusive qualitative method of measuring the density variations in a fluid. The density of a fluid changes across a shock wave, and the different densities of the fluid result in different refractivity of light in connection with the Gladstone-Dale relation. This technique uses a mercuric oxide light source which shines on a parabolic mirror. This mirror collimates and reflects the light beam through the test section. The light that passes through the test section is reflected by another parabolic mirror onto a knife edge. The knife edge is placed at the focal point of the beam and blocks any light refracted in its direction. The

result are dark and white regions corresponding to positive and negative gradients which are projected on a screen by a mirror behind the knife edge. For the experiments, this technique was useful in the identification of shock waves, locating their points of origin and impingement



and confirm the start/unstart of the tunnel, all of which together helped in modifying the experimental set ups accordingly.

4.3 Surface Flow Visualization

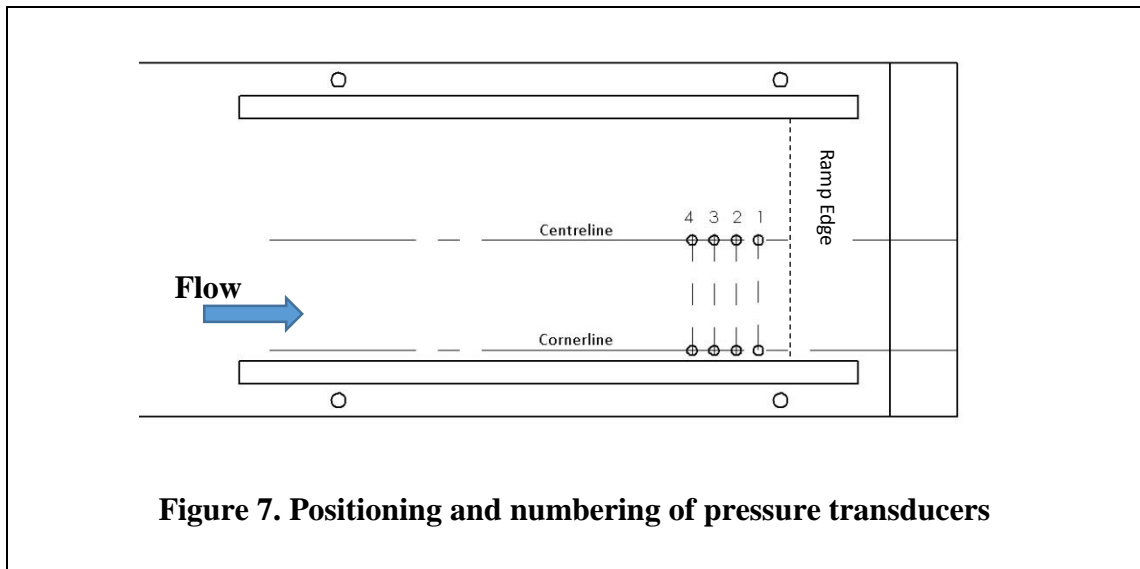
Surface Flow Visualization was performed on the surface of flat plate and fences, to examine the corner/junction boundary layer, flow separation features and the spanwise variation of the separation region. This method observed the movement of the shear forces of the viscous flow on the oil mixture spread on the surface of the set up and provided a visual image of the junction boundary layer and the separation effects. The oil mixture was made of aluminum oxide and kerosene oil mixed to achieve the desired viscosity. The set up was painted black before the experimental runs, using the flat black spray paint from Krylon, in order to allow for maximum contrast between the surfaces and the white oil flow. It was observed that the best result was obtained when flow visualization was done on a two coats of freshly dried paint (dried for approx. 4 hours) with a mixture of ratio 1:1. The oil flow images were recorded after the runs, assuming that the mixture had dried before tunnel shut down.

4.4 Unsteady Pressure Measurements

Pitot pressure measurements for the flat plate boundary layer experiment were taken with a high frequency transducer (Kulite Semiconductor Products, Inc., ITQ-1000-15 G). The signals were acquired at a rate of 100 Hz with a data acquisition board (National Instruments 9215) installed on a personal computer and read through a LabVIEW VI.

Fluctuating wall-pressure measurements are made in, and just downstream of, the intermittent region of the corner SBLI. Four transducers were placed along the centerline (50.8 mm from the longest edge of the flat plate) and corner (3.175 mm from the surface of the fence that is a part of the measurement domain) such that the transducer closest to the ramp was at a distance of 3.3 mm from the edge of the ramp and the rest were placed at 6.3 mm consecutively. The

pressure fluctuation measurements were made using a high frequency response transducer (Kulite Semiconductor Products, Inc., model XCQ062-15A). The transducer has a nominal diameter of 1.7 mm. The natural frequency of the membrane is 200 kHz. Perforated screens above the diaphragm protect the transducer from being damaged by the dust particles in the flow. The signals from the pressure transducers were filtered at 50 kHz using Vishay Measurements amplifier (Model 2350). The filtered signals were digitized at a rate of 50 kHz with a data acquisition board (National Instruments 9215) installed on a personal computer and read through a LabVIEW VI.



4.5 Auxiliary Experimental Set up

Initially, prior to starting the experiments, a hole of diameter 114.3 mm was drilled in the roof of the wind tunnel in order to suspend flat plates with variations as per need. A circular

aluminum plug was then designed that covered this hole and held the experimental set ups. A key feature of this plug was that its base could be detached and replaced with another one of a different design. This, in future, would help in mounting set ups with different configurations. A pair of struts held the flat plate from the base of the plug. The struts were machined to a width such that the set ups were above the boundary layers that formed on the walls of the wind tunnel during its operation. Also, a set of middle mount and centre mount was designed to shield the pressure transducers during wall static pressure measurements. A schematic showing the plug with the detachable base, mounting struts, middle and the corner mount is shown in figure 8.

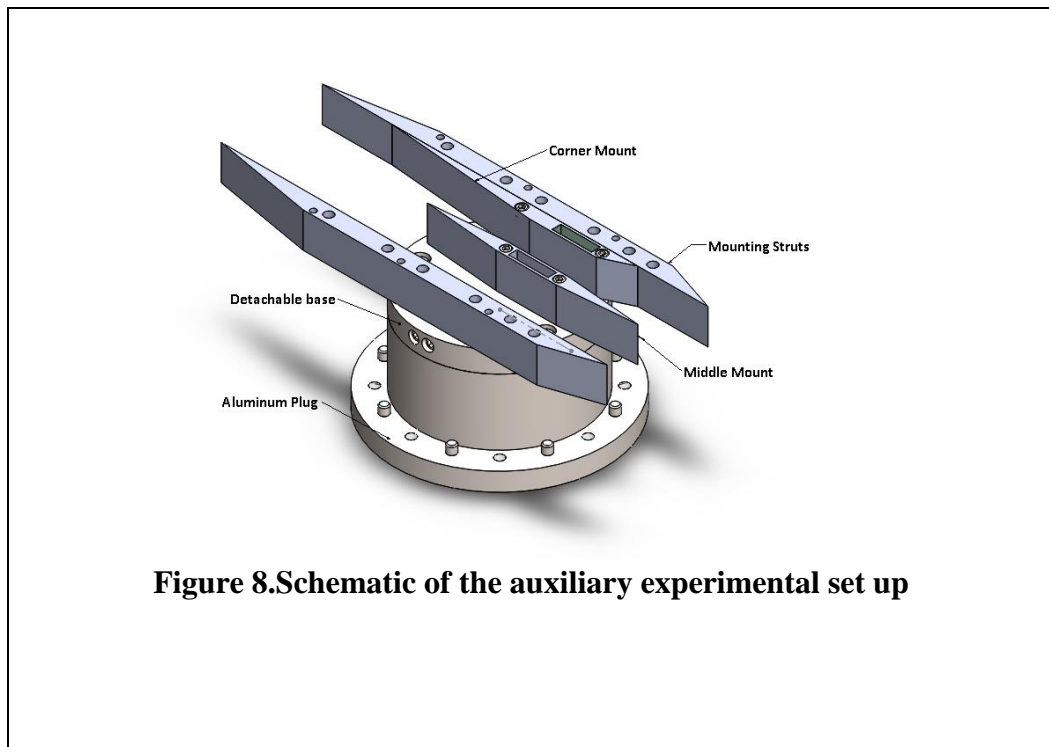


Figure 8. Schematic of the auxiliary experimental set up

CHAPTER-5. FLAT PLATE BOUNDARY LAYER MEASUREMENT

As the flat plate was an important part of the experimental set up on which the boundary layer developed and separated in the SBLI, it was essential to locate a point from the leading edge of the plate where a boundary layer of an optimum thickness developed, that would be suitable to undergo separation in the later experiments. This would also help in positioning the compression ramp on the plate accordingly. Hence as a supporting experiment, the thickness of the turbulent boundary layer on a flat plate was calculated the test Mach numbers of 2.5 and 3.3.

5.1 Experimental Setup

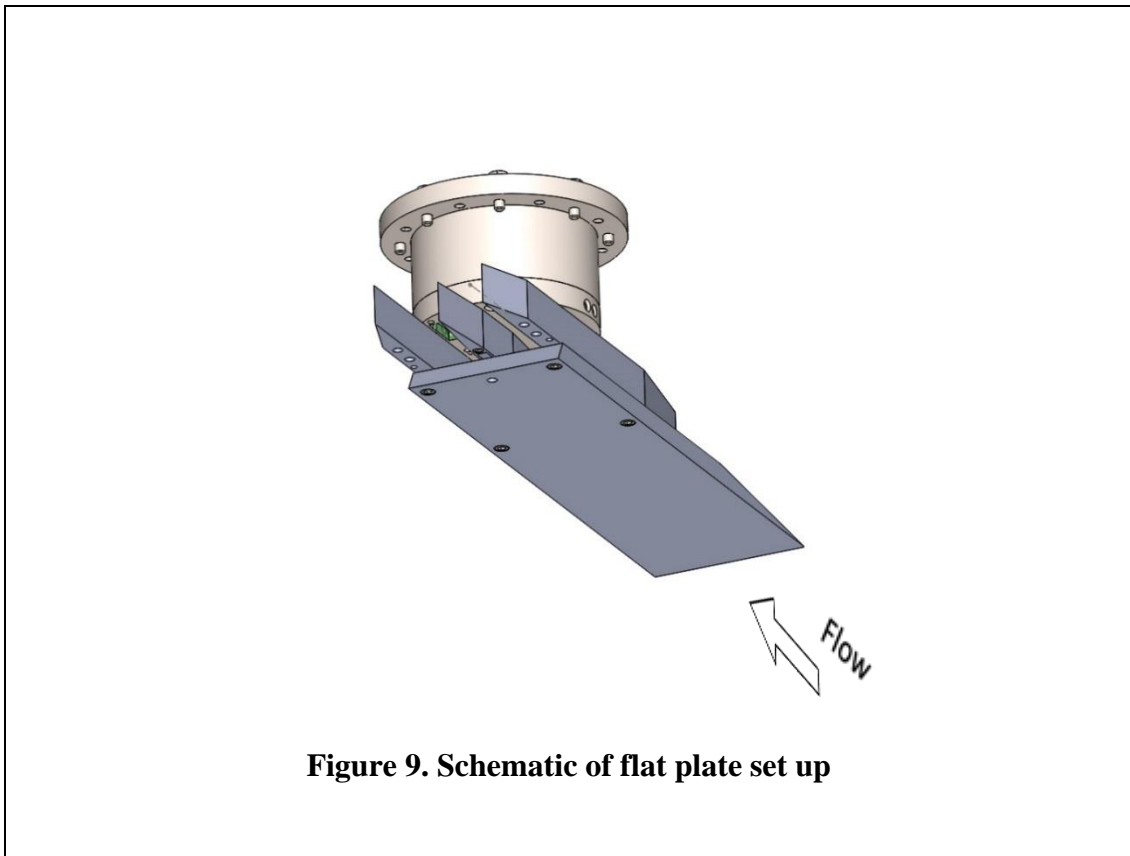
The flat plate was a rectangular piece of low carbon steel (AISI 1018) 101.6 mm (4") in width and 12.7 mm (1/2") in thickness, that was machined to a length of 355.6 mm(14"). A through hole drilled at the other end of the plate allowed the pitot probe to be inserted through it. It was installed onto the mounting struts using socket head screws. In order to minimize the formation of extraneous shocks, the end of the plate that would face the incoming flow was given a small angle by machining down one of the surfaces. Additionally, the same side on the other end was also machined to an angle. The heads of the screws were also flush with the surface of the plate to reduce undulations during pitot pressure measurements.

The pitot probe was a right angled copper tube with an inner diameter of 1.5875 mm (1/16") inner diameter enclosed in a stainless steel tube (6.35 mm (1/4") inner diameter). The machined end was on the shorter arm and would be exposed to the incoming flow. To avoid the formation of shocks in front of the arm perpendicular to the flow, the longer arm was glued to the outer

tube in such a way that 25.4 mm (1") of its length from the right angled end a strip of stainless steel filed on one side and glued onto the copper tube. In the complete set up, the probe was located at approx. 304.8 mm (12") from the leading edge of the plate,

A linear actuator from Newmark Elements installed on the aluminum plug held the pitot probe.

The schematic and the complete set up are shown in the figures 9 and 10 respectively.



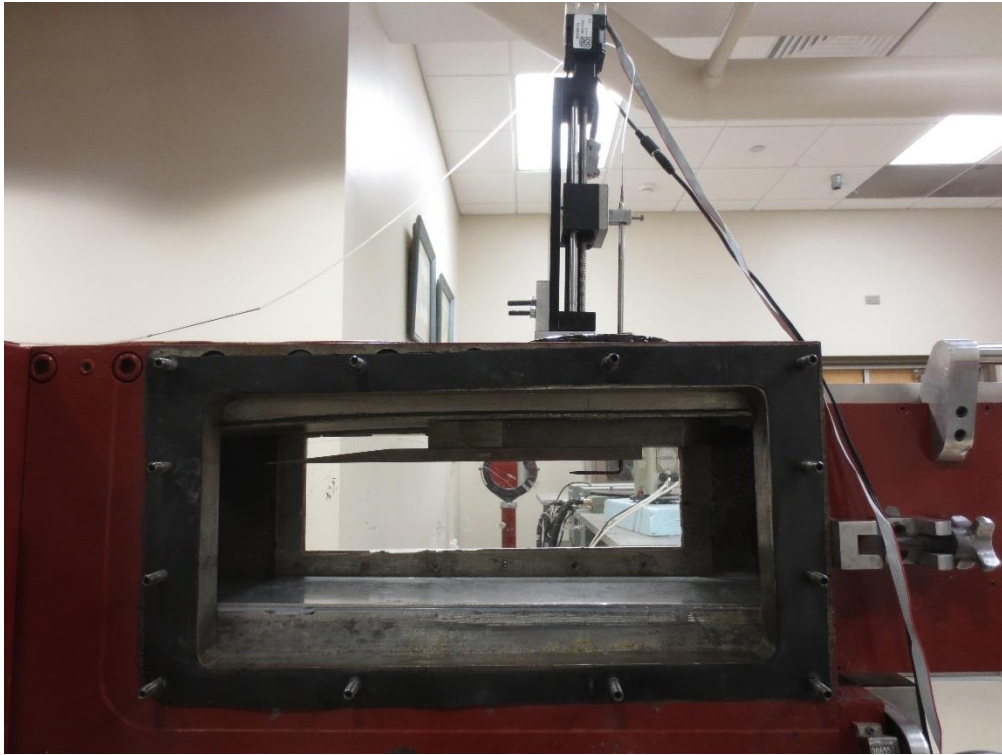


Figure 10. A view of the flat plate set up in the wind tunnel

5.2 Experimental procedure

The thickness of the boundary layer was determined at the test Mach numbers of 1.3, 2.5 and 3.3. The pitot pressure measurements were taken at every 1 mm, from the surface of the plate, using the linear actuator to move the probe. At the closest point when the arm of the probe touched the surface of the plate, the axis of the pitot head was offset by 2 mm. Hence, this allowed the boundary layer measurements to be taken only till a maximum distance of 2 mm

from the surface of the plate. The procedure to calculate the fluid velocity from the pitot pressure is as following:

1. The free stream Mach number is used to calculate the static pressure using the isentropic relations

$$\frac{p_o}{p} = \left(1 + \frac{\gamma - 1}{2} M^2\right)^{\frac{\gamma}{\gamma - 1}}$$

- 1) Since the static pressure is constant throughout the thickness of the boundary layer at a particular stream wise distance, the ratio of the measured pitot pressure to the static pressure yields the Mach number at that point in the boundary layer using the same relation as in step 1.
- 2) The flow static temperature is calculated using the isentropic relation

$$\frac{T_o}{T} = \left(1 + \frac{\gamma - 1}{2} M^2\right)$$

- 3) The calculated flow static temperature yields the speed of sound from the relation

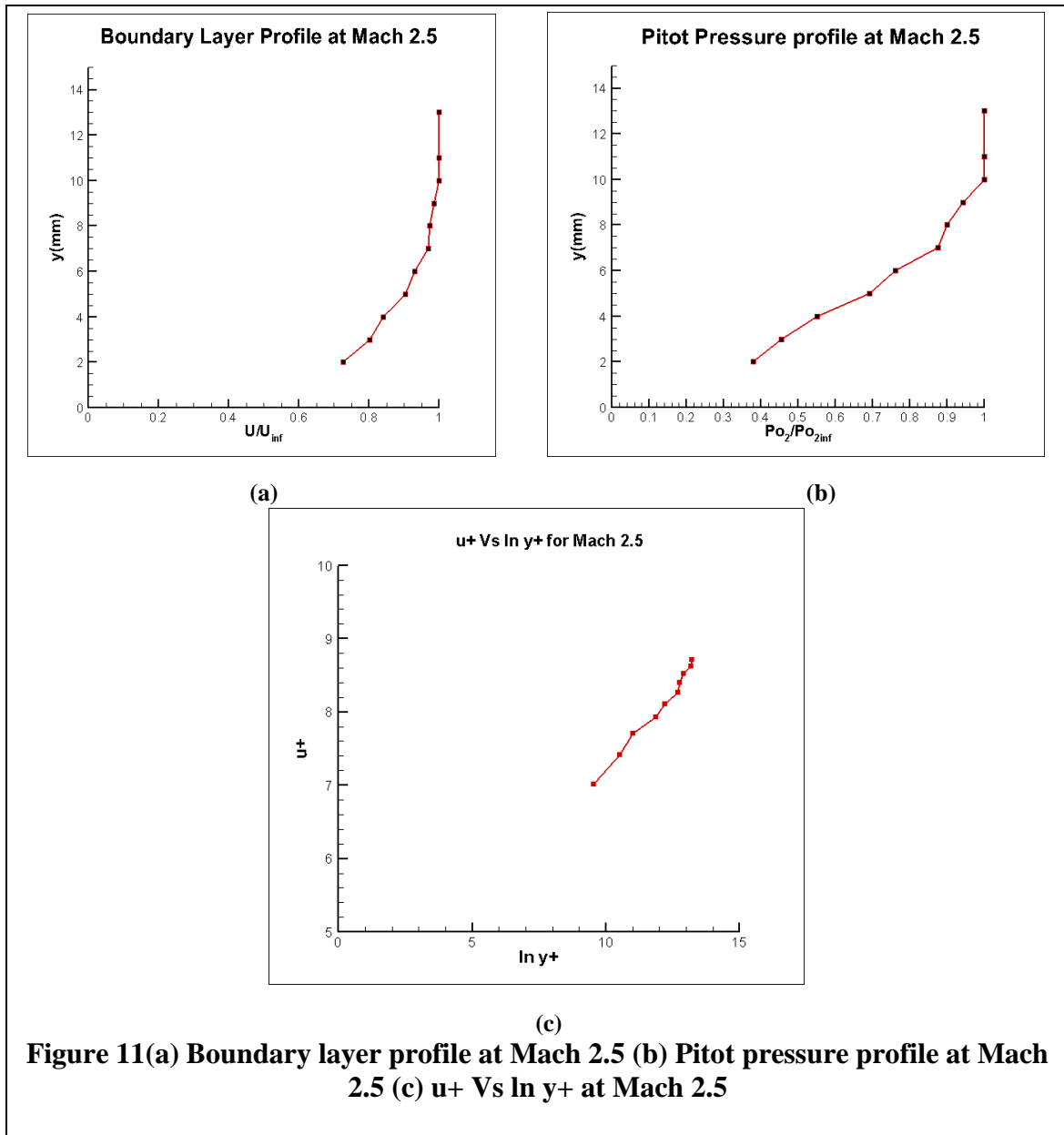
$$a = \sqrt{\gamma RT}$$

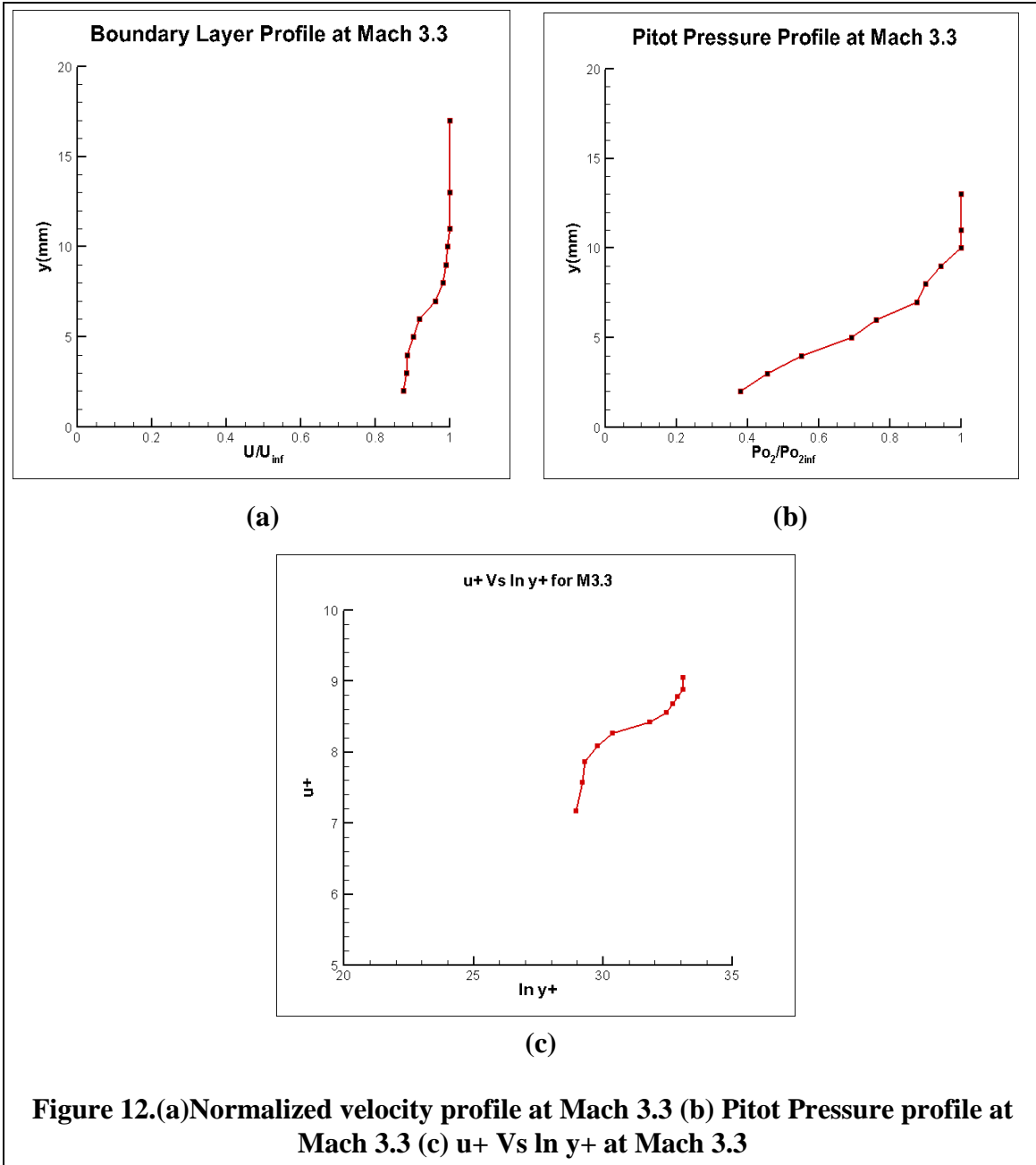
- 4) This is used to calculate the fluid velocity using the relation

$$u = \frac{M}{a}$$

The procedure was repeated for all the points at which the pitot pressure was measured and for the Mach numbers at which the experiments were conducted. The errors in the pressure measurements may have been due to the vibration of the arm of the probe due to the high

velocity of the fluid around it and also a slightly skewed orientation of the head of the probe with respect to the flow as the probe was aligned manually.





5.3 Results and Discussion

Boundary layer determination at Mach numbers of 2.5 and 3.3 provided information about the upstream boundary layer conditions which is very important in the understanding of SBLI. The boundary layer profiles indicate the ability of the flow to undergo interaction and separation. The normalized velocity profiles are shown in figures 11 and 12.

Table 1. Incoming Boundary Layer Data

Mach No.	θ (mm)	Re_θ	$\delta_{99\%}$ (mm)	δ^* (mm)	τ_{wall} (N/m ²)
2.5	0.677	43972.8	10	2.772	228.838
3.3	0.665	296446	12	2.454	126.294

CHAPTER-6. SBLI IN EXPERIMENTAL SET UP

6.1 Incident shock reflection method

6.1.1. Experimental Setup

Among the several methods available to generate SBLIs, the incident shock-reflection was chosen at first to study the corner SBLI. With the length of the plate to obtain an optimum turbulent boundary layer (approx. 10 mm) known, a new set up was designed wherein the flat plate was slotted at two positions, parallel to its longest side, to accommodate a pair of fences. The fences when installed in the slots were perpendicular to the plate and ran along its full length projecting some distance outward at both the end. As the fluid flowed over this set up of the plate corner/junction boundary layer would start growing from the leading edge of the plate at the intersection of the surface of the plate and the fence attaining the maximum thickness at the trailing edge of the plate. This is shown in figure 13.

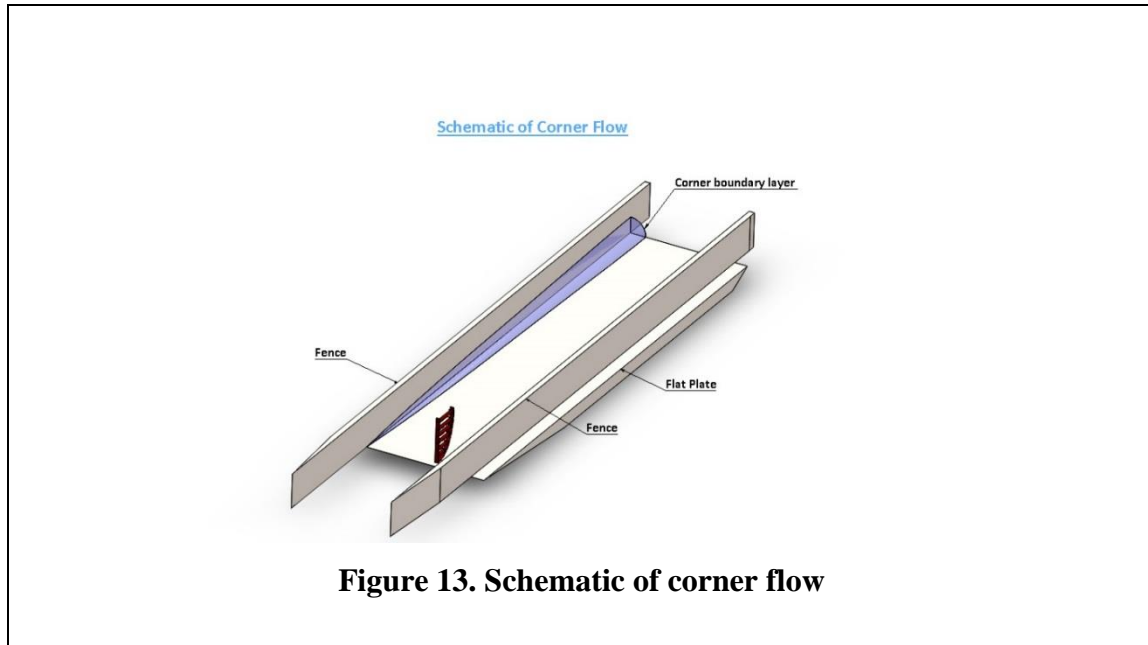


Figure 13. Schematic of corner flow

This flow would be separated by an impinging incident oblique shock wave formed by a compression ramp of angle 8° . The compression ramp spanned the width of the wind tunnel. It was installed on the floor of the test section using a pair of supports. It could be positioned at different stream wise positions using the screw holes along the base of the windows. This gave a control over the strength of the SBLI shock impinging region could be shifted upstream or downstream in order to separate the boundary layer of the optimum thickness. The SBLI was qualitatively measured by surface flow visualization and schlieren imaging.

6.1.2. Surface Flow Visualization

Flow visualization of this method is shown in Figure 14. Although the flow visualization was of poor quality, it allowed some structures of the separation to be identified in the region of the SBLI. The direction of flow is from top to bottom. The line of separation is seen as the region

where the mixture builds up as a white band at the top of the image. This is because the flow was no longer moving downstream. The streaks of white lines post this region are seen to move upstream suggesting flow reversal. The location from which the streamlines start moving downstream again is the line of re attachment. A vortex is seen near the right side fence. This highly suggested the three dimensionality of the flow although it did not confirm the separation of the corner boundary layer, as a similar vortex was not seen near the left fence.

6.1.3. Schlieren Imaging

The reason behind the poor quality of the flow visualization was investigated by repeating the experiment and by running a schlieren imaging simultaneously. Through schlieren, it was

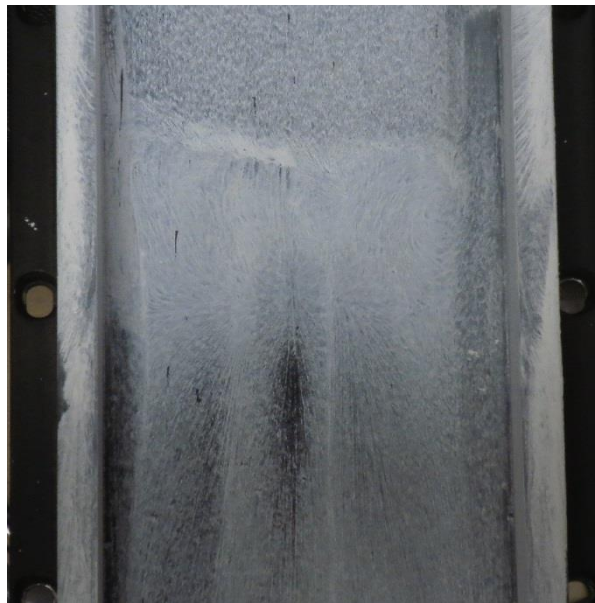


Figure 14. Surface flow visualization with incident shock method

learnt that along with the incident shock wave, there was an extraneous shock wave that originated near the foot of the supports and disturbed the flow field. Initially, it was thought that the blockage offered by the compression ramp due to its span may be the cause behind the generation of this extraneous shock. Thus, its cross-sectional area was minimized by reducing its span, so that the air could flow around it. However, on repeating the experiment, the extraneous shock was still observed. As reason behind its origin could not be traced, it was decided that this method of investigating the SBLI would be discontinued and other options had to be explored.

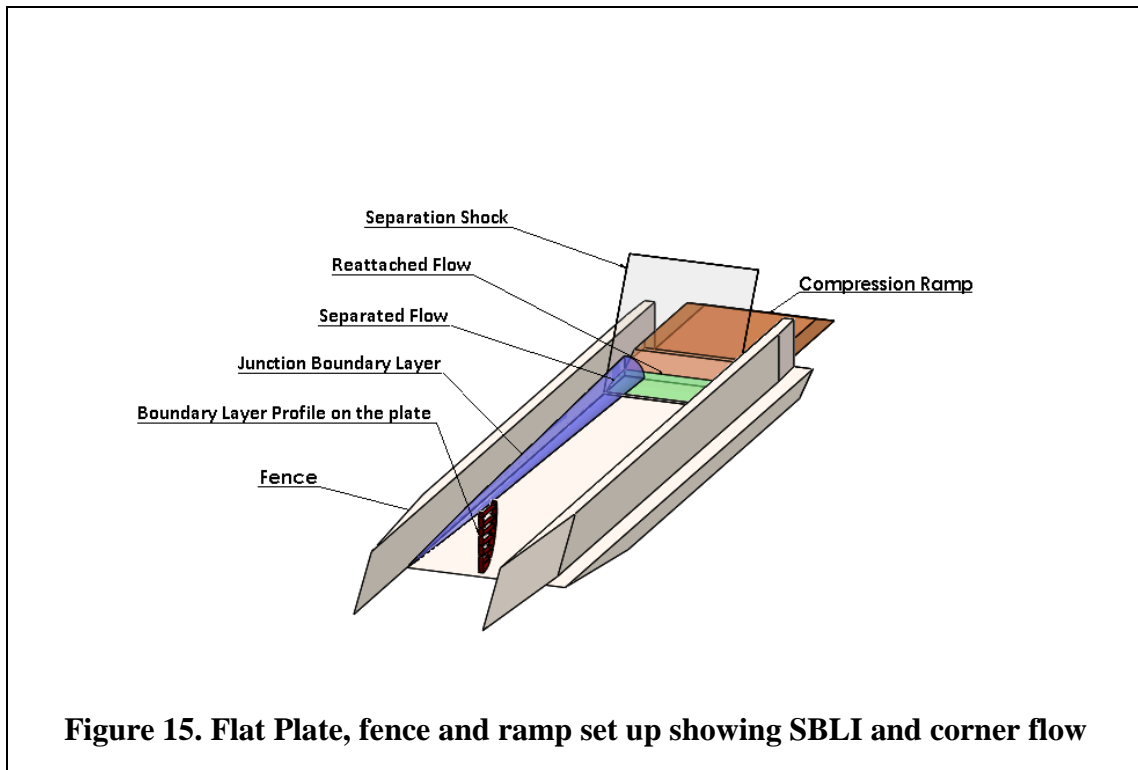
6.2 Flow Separation by compression ramp

6.2.1 Experimental setup

The present set up was suitable for the installation of a compression ramp using which an oblique shock wave could be generated. On installing it on the flat plate itself, the overall blockage in the wind tunnel could be brought down, thereby lowering the occurrence of extraneous shocks as in seen in the previous case and chances of tunnel unstart. Additionally, the set up was overall a one piece assembly now that could be handled easily.

A compression ramp was separately designed for this purpose, with a combination of 12° and 16° angles for testing with different shock strengths. It was installed in between the two fences downstream of the flat plate such that the edge protruded to approx. 50.8 mm (2") into the plate. This was intended to separate a boundary layer of optimum thickness. The schematic of the SBLI due to a compression ramp is shown in figure 15. Three sets of experiments at two test Mach numbers were conducted on this set up. The first one was carried out without the compression ramp (baseline flow). Next, flow separation was studied by testing with 12° and

16° angles individually. In all the cases, surface flow visualization was done and static pressure measurements were taken along the centre and the corner separately. Thus, a complete database, both qualitative and quantitative, was accumulated of the whole flowfield which helped in characterizing the corner SBLI.



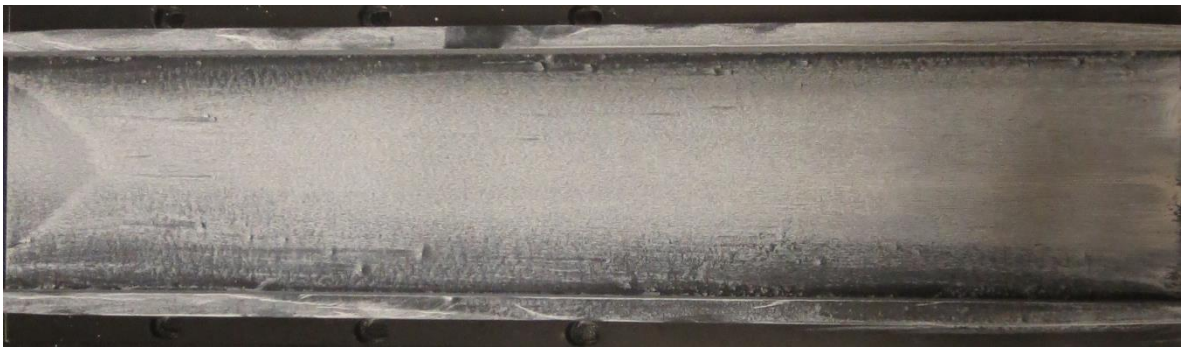
6.2.2. Baseline Flow

Flow over the set up without the installation of the compression ramp is termed here as baseline flow. Flow visualizations was first conducted at both the testing Mach numbers to view the corner boundary layer over the flat plate. It was then followed by the static pressure

measurements with the same configuration to confirm the high frequency oscillation characteristic generally observed in baseline flow.



(a)



(c)

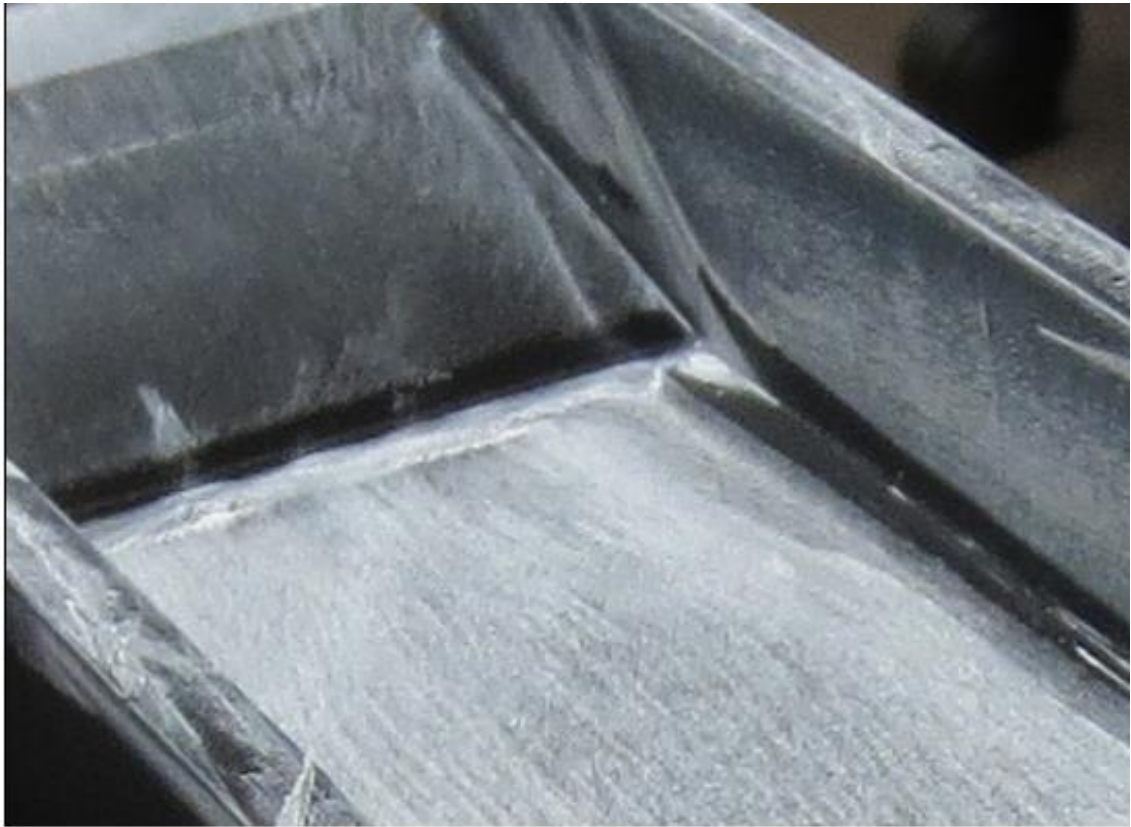
Figure 16. (a) Flow at Mach 2.5 (b) Flow at Mach 3.3

Figure 16. shows the flow visualization of the baseline flow at Mach numbers of 2.5 and 3.3. The direction of flow in the figures is from right to left. The black region that is seen to develop at the upper and lower corners both along the length of the plate is the corner boundary layer. On comparing the figures of the two Mach numbers, the boundary layer is seen to grow more and occupy a higher spanwise portion of the plate in the case of Mach 3.3. This indicates that the corner boundary layer like the 2-D boundary layer at a particular streamwise point is of higher thickness at a higher Mach number. A triangular feature is seen at the end on the left side of the plate. The reason behind the occurrence of this feature could not be found out. It may have been caused by the extraneous shocks formed due to the surface irregularities on the tunnel floor impinging this region. However, it is clearly visible that it did not separate the flow in that region due to which it was ignored in the later experiments. Moreover, the flow to be separated would be far upstream of this region after the installation of the compression ramp at this end which made it safe to neglect it.

6.2.3 Results and Discussion-Shock induced separation with 12° and 16° compression ramp

6.2.3.1 Surface Flow Visualization with 12° ramp (Mach 2.5)

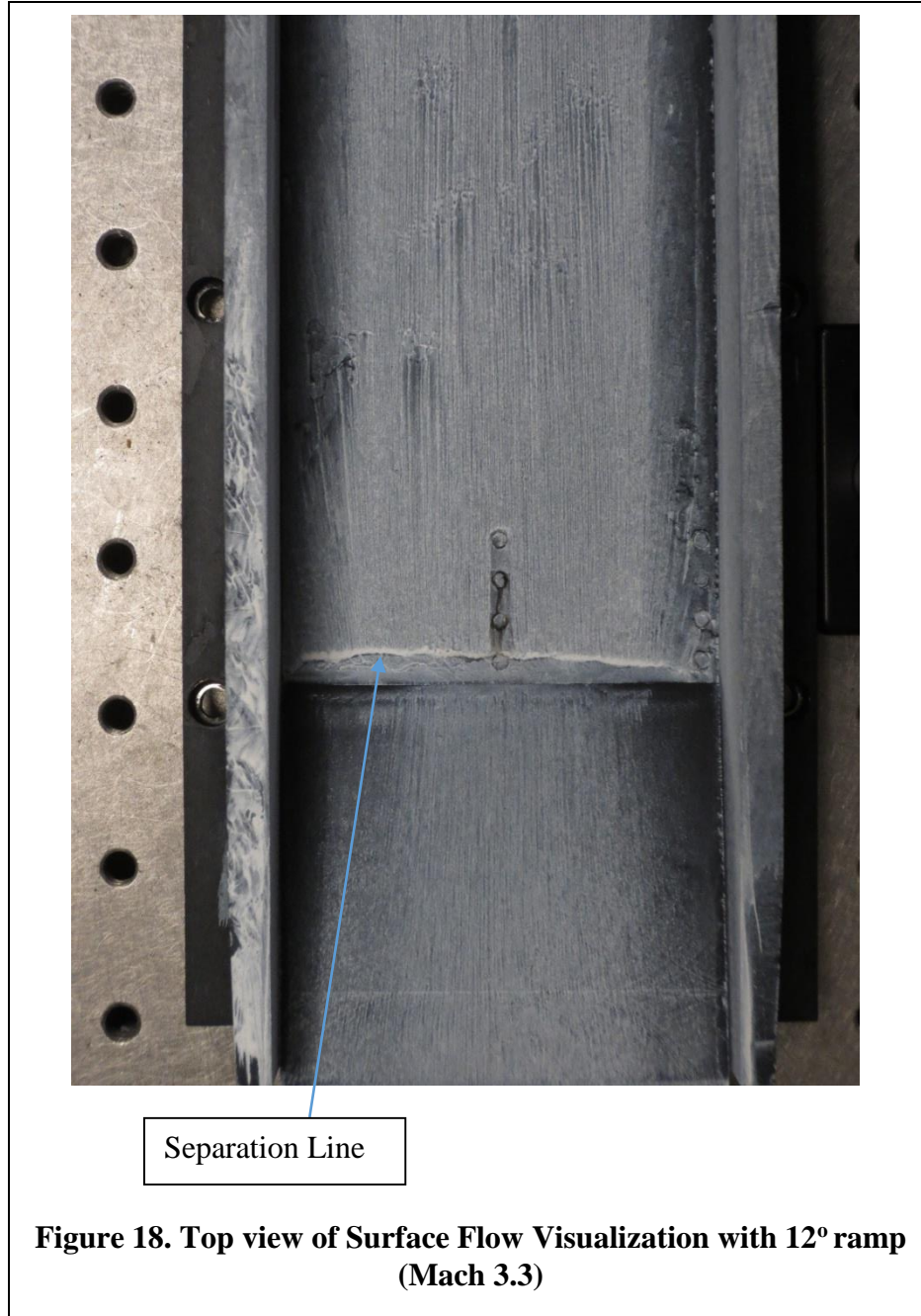
Figure 17. Surface Flow Visualization with 12° ramp (Mach 2.5) (a) side view (b) isometric view (c) top view



(b)

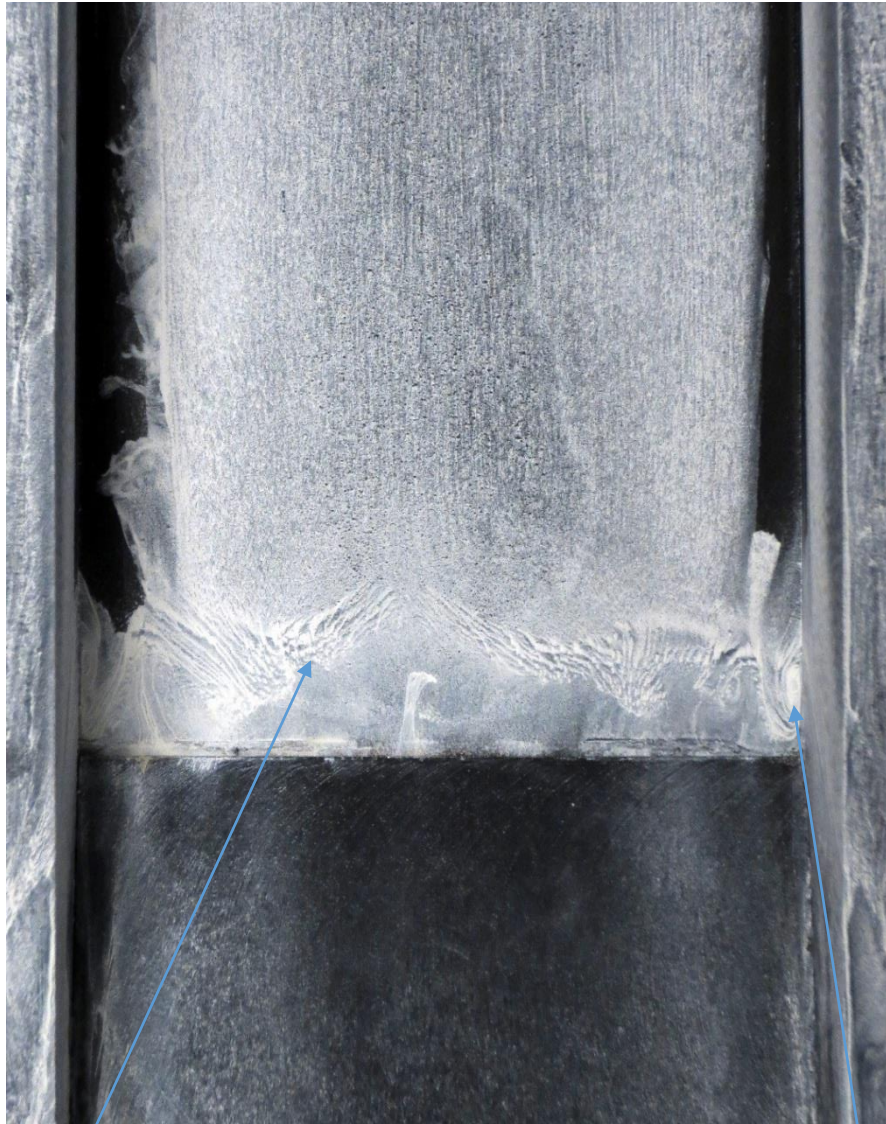


6.2.3.2 Surface Flow Visualization with 12° ramp (Mach 3.3)



6.2.3.3 Surface Flow Visualization with 16° ramp (Mach 2.5)

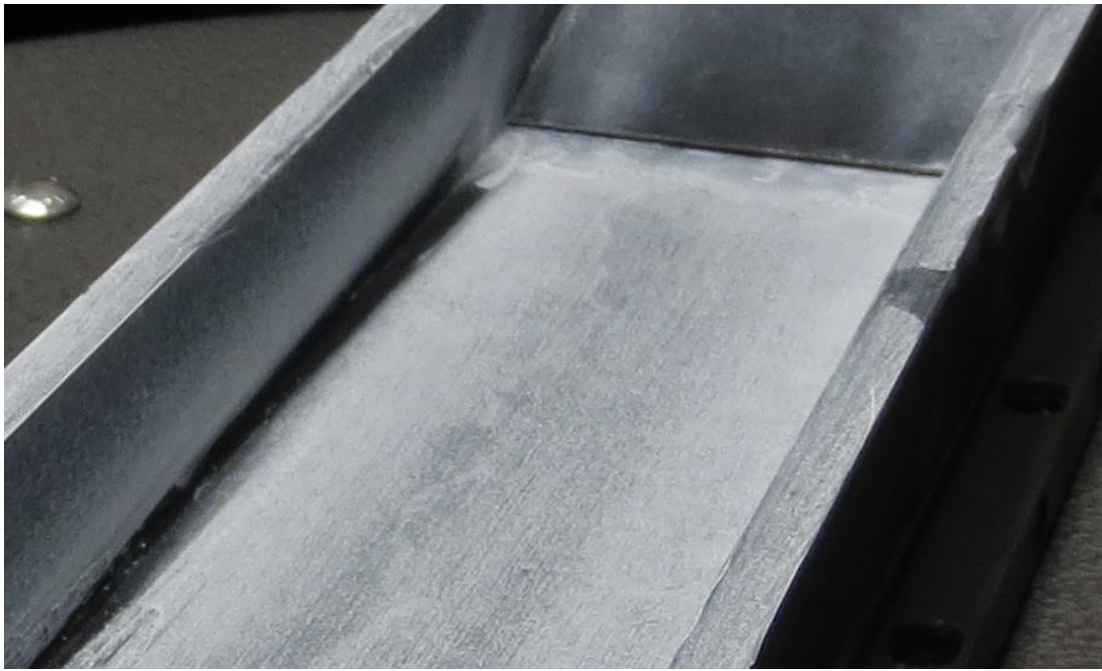
Figure 19. Surface Flow Visualization with 16° ramp (Mach 2.5) (a) top view (b) isometric view (c) side view



(a)

Separation Line

Counterclockwise Vortices



(b)



(c)

6.2.3.4 Surface flow visualization with 16° ramp (Mach 3.3)

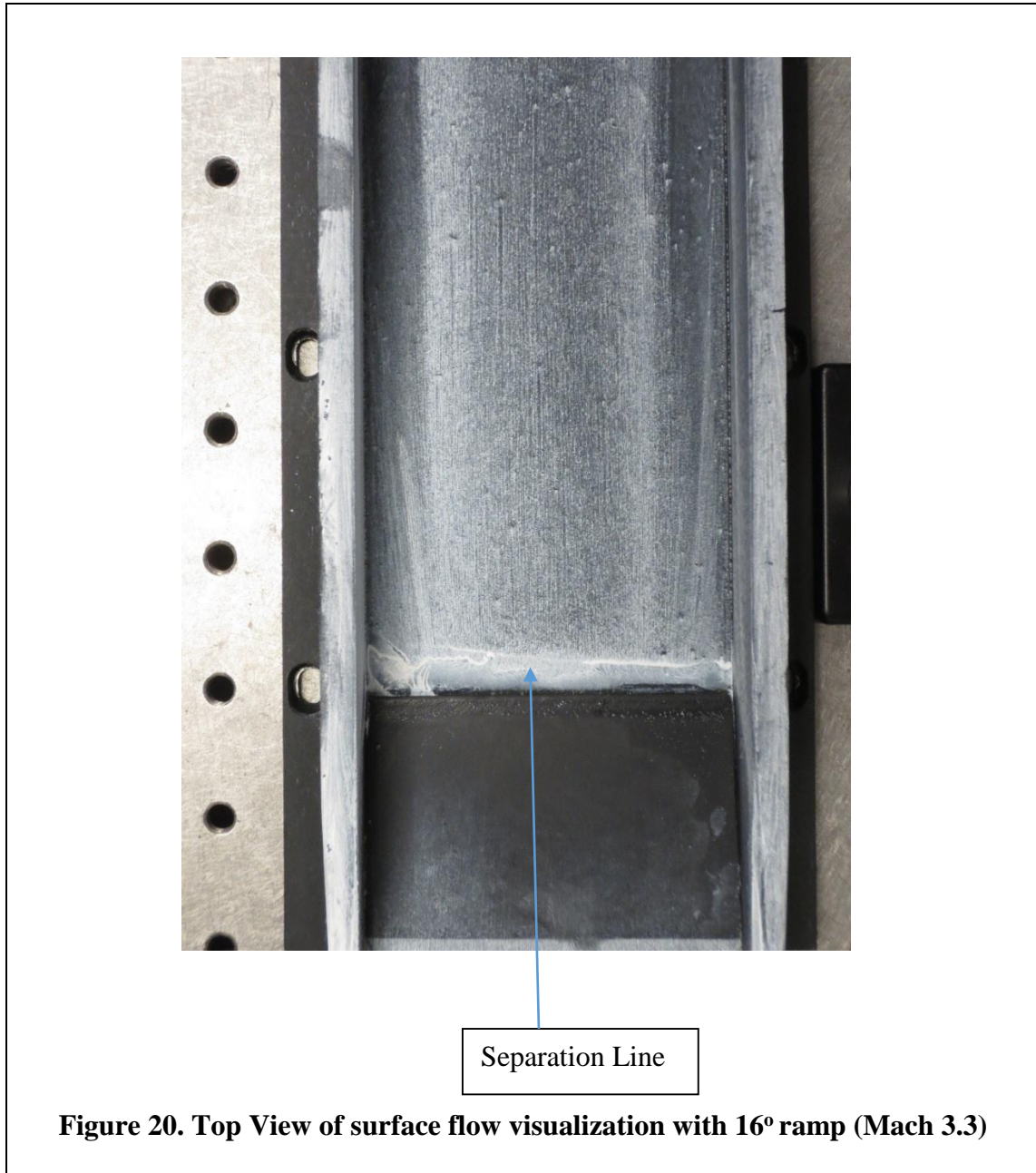
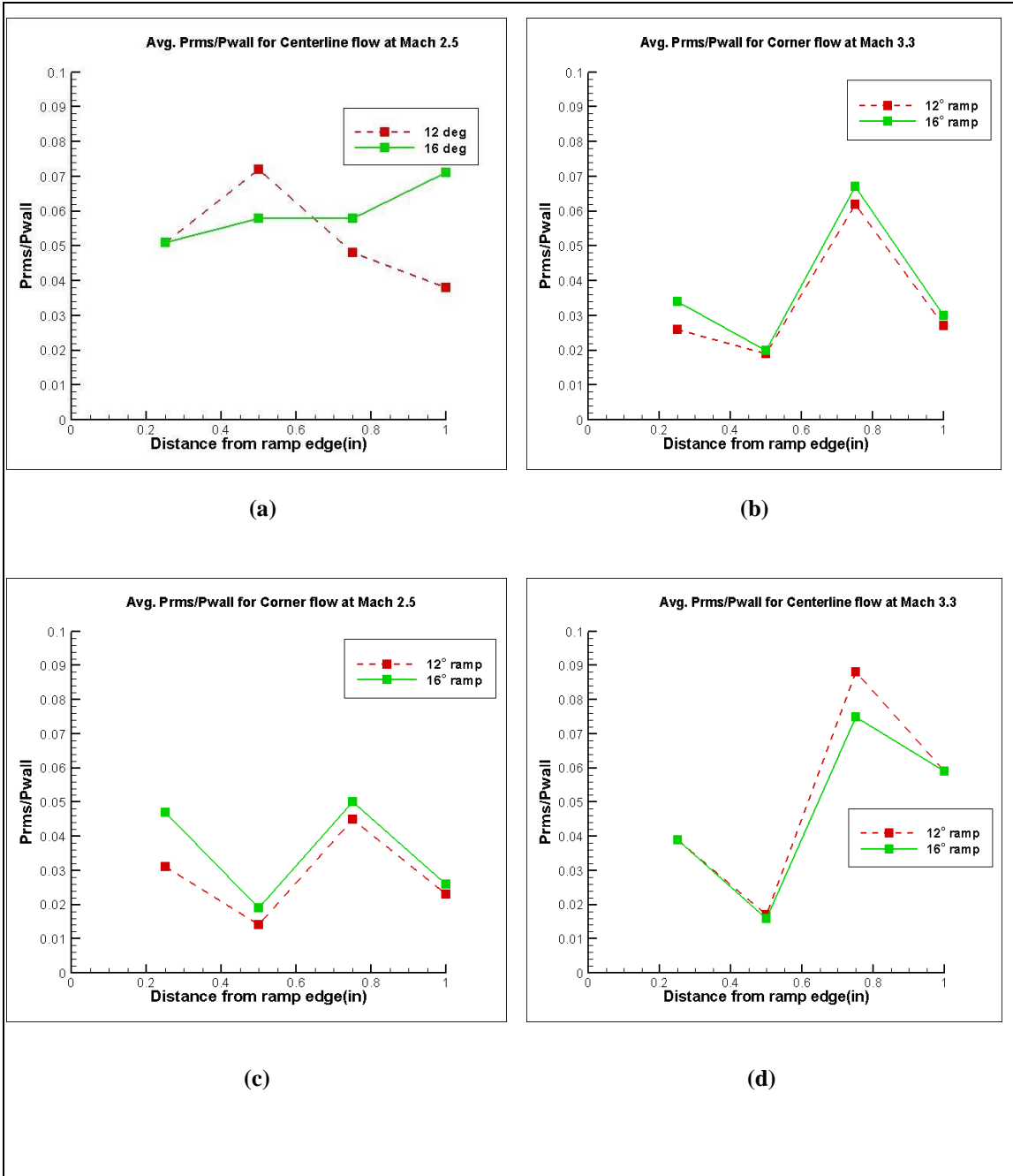


Figure 17 and figure 18 show the flow visualization of SBLI with a 12° ramp at Mach 2.5 and Mach 3.3 respectively. Figure 19 and figure 20 show the flow visualization of SBLI with a 16° ramp at Mach 2.5 and Mach 3.3 respectively. The flow direction is from top to bottom in images that represent the top and is from right to left that represent the side views. Corner boundary layer on the plate and the fence is seen as a growing black region in all the figures. Many of the flow structures that are part of SBLI can be identified in the above pictures. In figure 17(c), 18, 19(c) and 20, at some distance upstream from the ramp, the flow streamlines end abruptly. This is the line of flow separation. The region in between this line and the ramp is occupied by the separation bubble throughout the span till the edge of the corner boundary layers at either corners. In figure 17(c), it is observed that the line of separation across the span is jagged that hints at the flow separation being three dimensional and has been highly influenced by the corner separation. Corner vortices that are counter-clockwise are observed at both the corners near the edge of the ramp. This confirms the 3-D nature of corner separation as suggested by Burton et al.(2010). Also, at a distance upstream of the corner on the top of 17(c), we observe streamlines entrain into a smaller channel of flow. This may be the onset of corner separation that has created a blockage effect for the incoming fluid and has occupied more spanwise distance. Comparing the figures 17(c) & 18 and 19(a) & 20, the streamwise distance of separation in the case of Mach 3.3 is less than that observed at Mach 2.5, which is as expected as the shock foot moves closer to the compression corner with increasing Mach numbers with the formation of a smaller separation bubble. It can be also seen that the flow separation at the same Mach number is higher for the larger angled ramp as seen in figure 17(c) and 19(a). Vortices were absent at either corners for both the angles at Mach 3.3 which

suggested a healthy corner boundary layer that could resist separation. The re attachment line over the ramp could not be observed in any of the cases.

6.2.4 Static Pressure Measurements

Figure 21. (a) Avg. Prms/Pwall for Centerline flow at Mach 2.5 (b) Avg. Prms/Pwall for Centerline flow at Mach 3.3 (c) Avg. Prms/Pwall for Corner flow at Mach 2.5 (d) Avg. Prms/Pwall for Corner flow at Mach 3.3



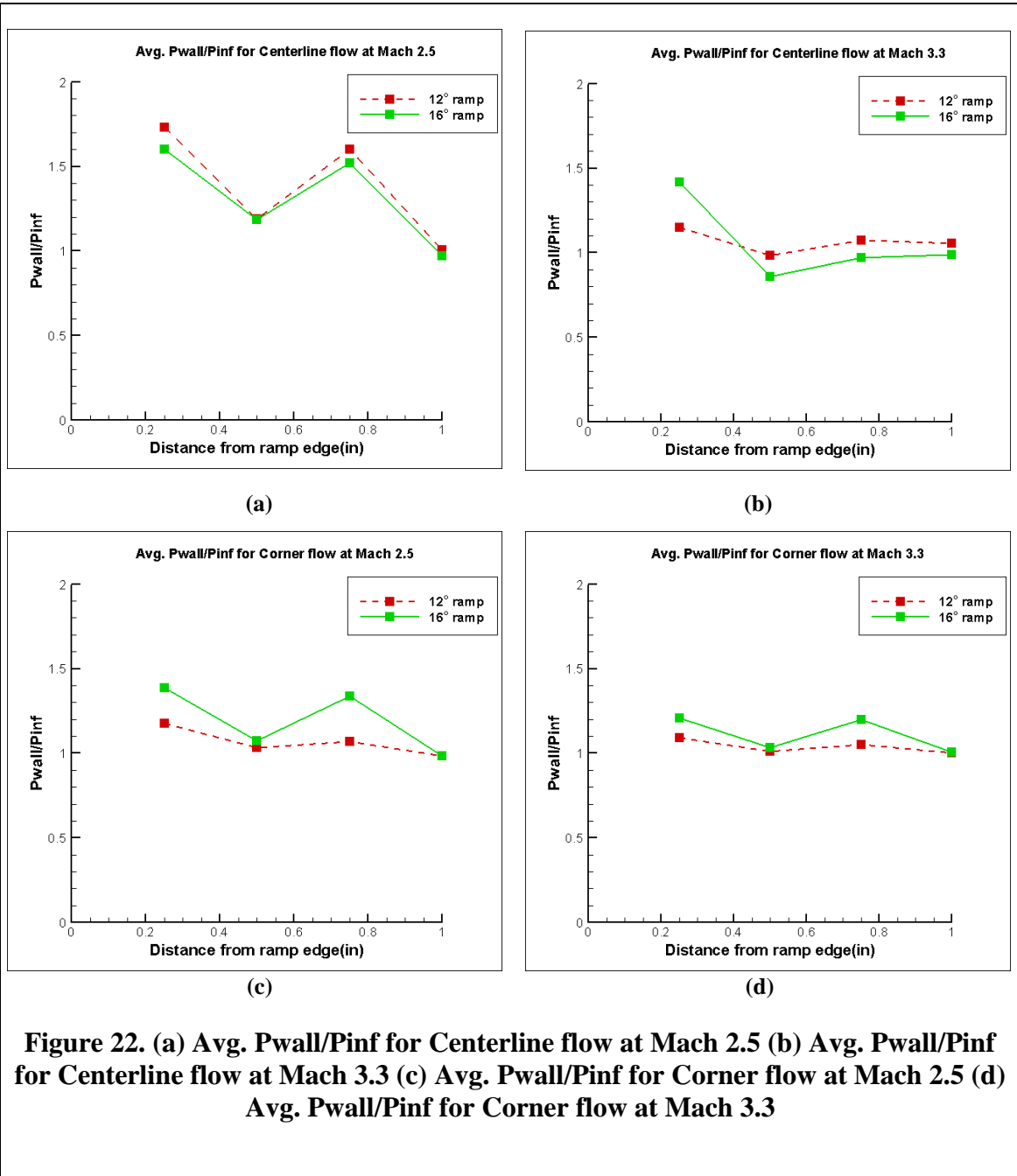
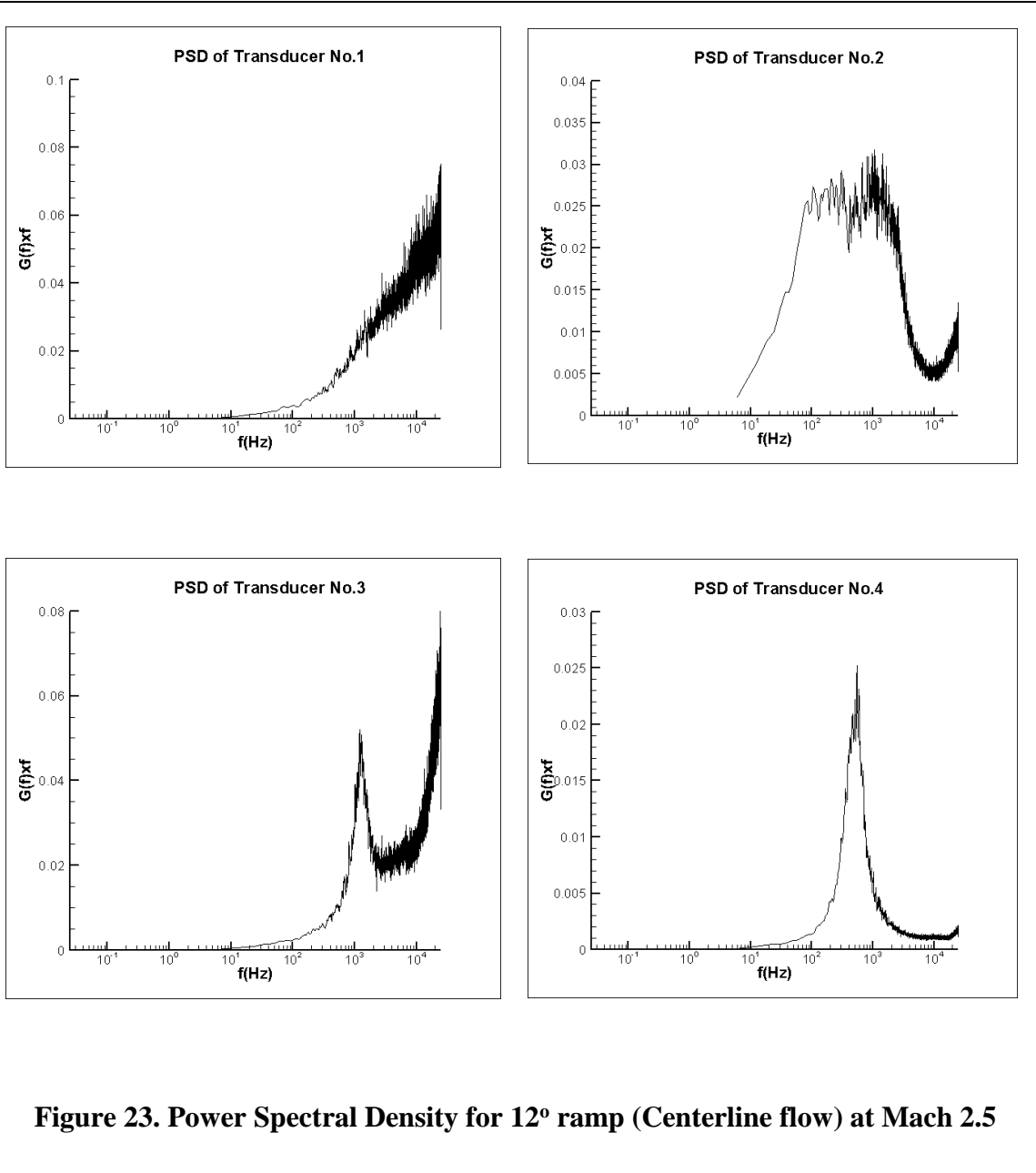


Figure 22. (a) Avg. P_{wall}/P_{inf} for Centerline flow at Mach 2.5 (b) Avg. P_{wall}/P_{inf} for Centerline flow at Mach 3.3 (c) Avg. P_{wall}/P_{inf} for Corner flow at Mach 2.5 (d) Avg. P_{wall}/P_{inf} for Corner flow at Mach 3.3

The average P_{rms}/P_{wall} values of the transducers for the 12° and 16° ramp is within 10 % which is in concurrence for an SBLI with an oblique shock wave. The lower ratios of the transducers for corner flow than centerline flow at Mach 2.5 for both the angles indicate smearing of adverse pressure gradients by the corner separation. At the same time, the trend for Mach 3.3 flow of both the angles is seen to collapse on another. Both types of trends are in good agreement with their respective flow visualization, as in Mach 2.5, vortices were seen due to corner separation while in Mach 3.3 no corner separation was observed.

The average P_{wall}/P_{inf} values of the transducers for the 12° and 16° ramp registers a higher deviation for transducers for centerline flow at Mach 2.5 than at Mach 3.3 which indicates an unsteady flow at the lower Mach No. Moreover, all the transducers except transducer no. 1 have a ratio approximately equal to 1 which for centerline and corner flow at Mach 3.3 for both the angles. This also suggests the closer proximity of the shock to the ramp due to the higher Mach No.



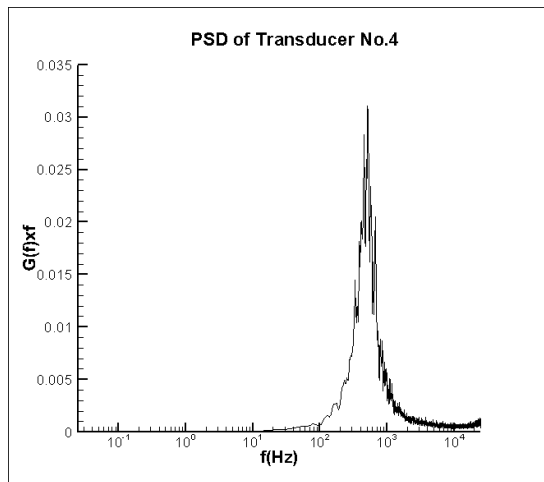
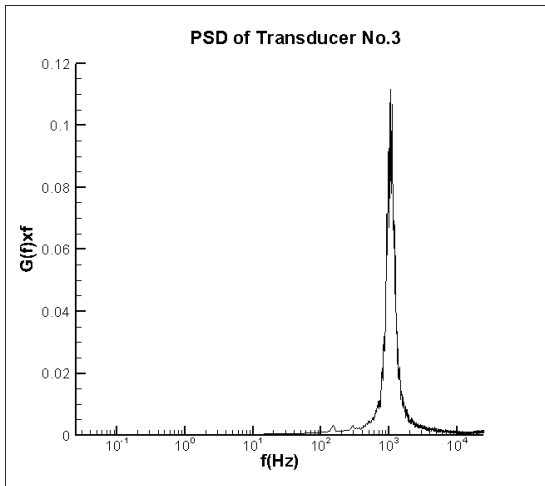
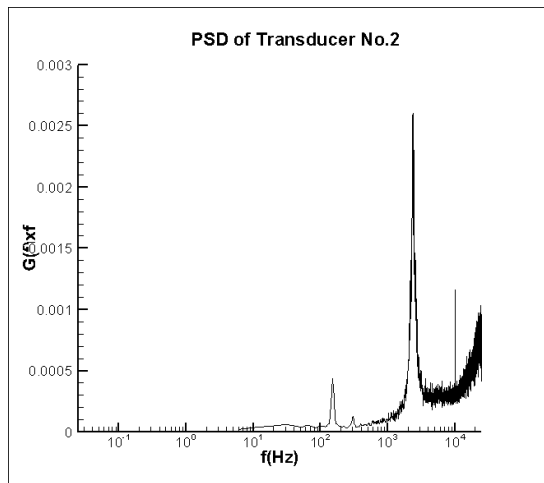
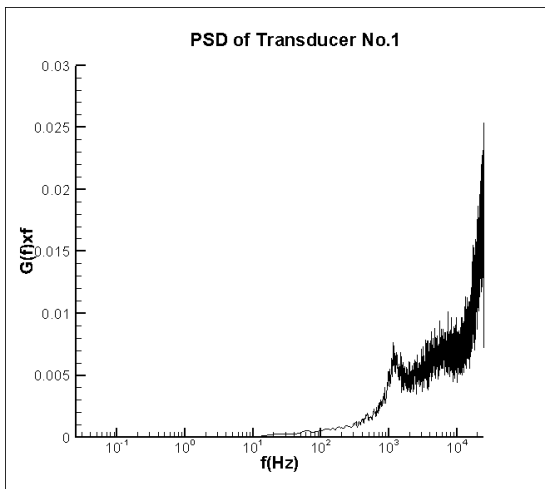


Figure 24. Power Spectral Density for 12° ramp (Centerline flow) at Mach 3.3

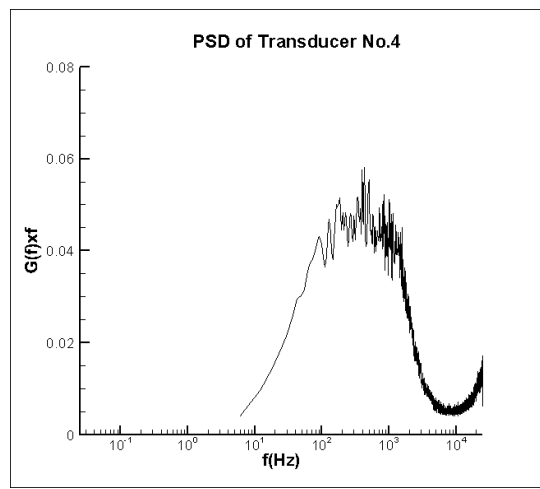
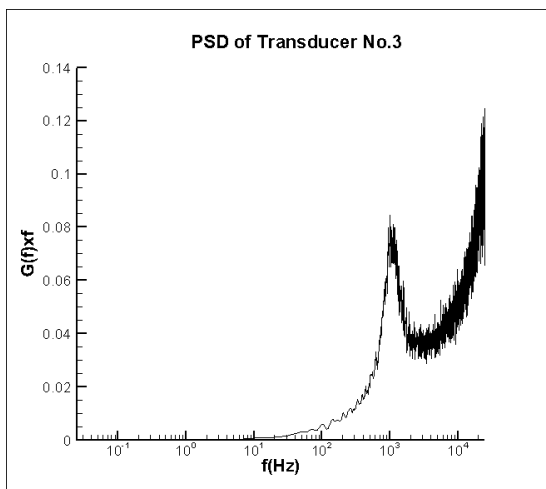
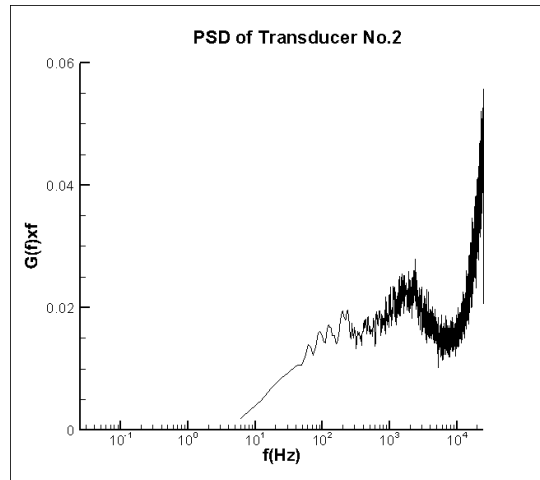
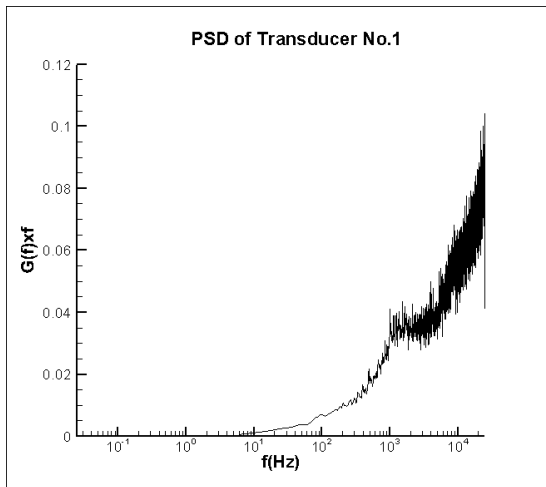


Figure 25. Power Spectral Density for 16° ramp (Centerline flow) at Mach 2.5

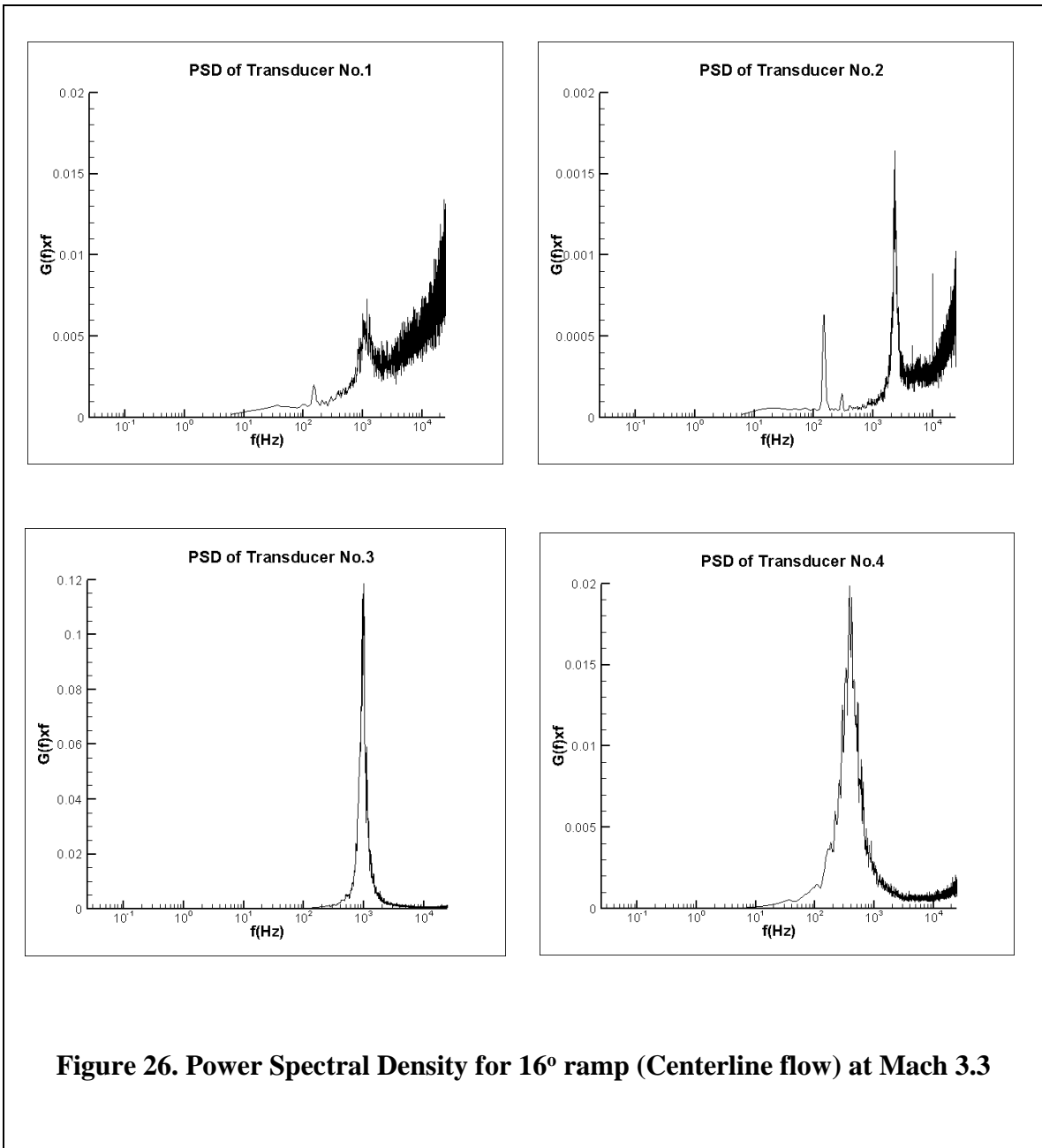


Figure 26. Power Spectral Density for 16° ramp (Centerline flow) at Mach 3.3

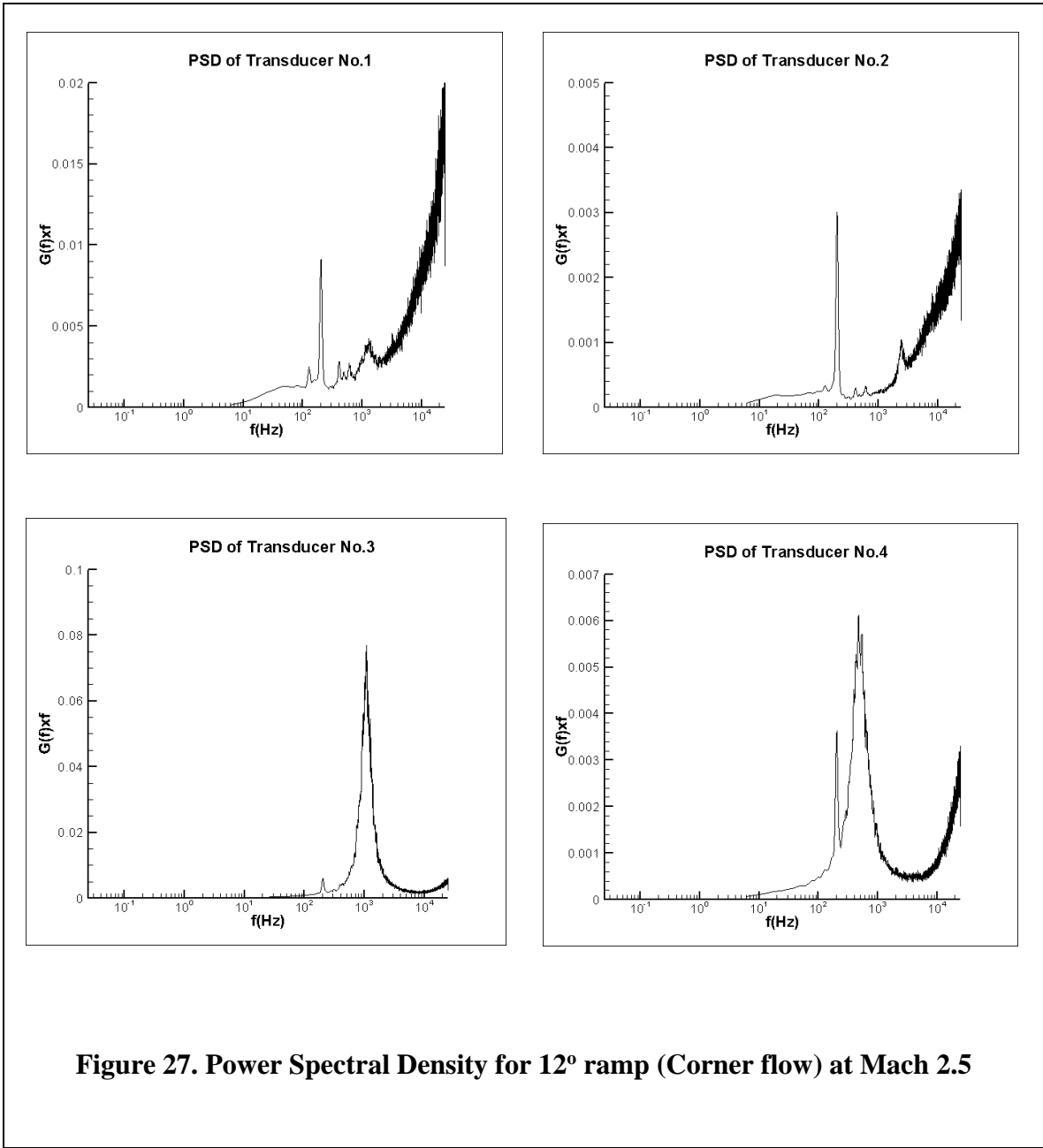


Figure 27. Power Spectral Density for 12° ramp (Corner flow) at Mach 2.5

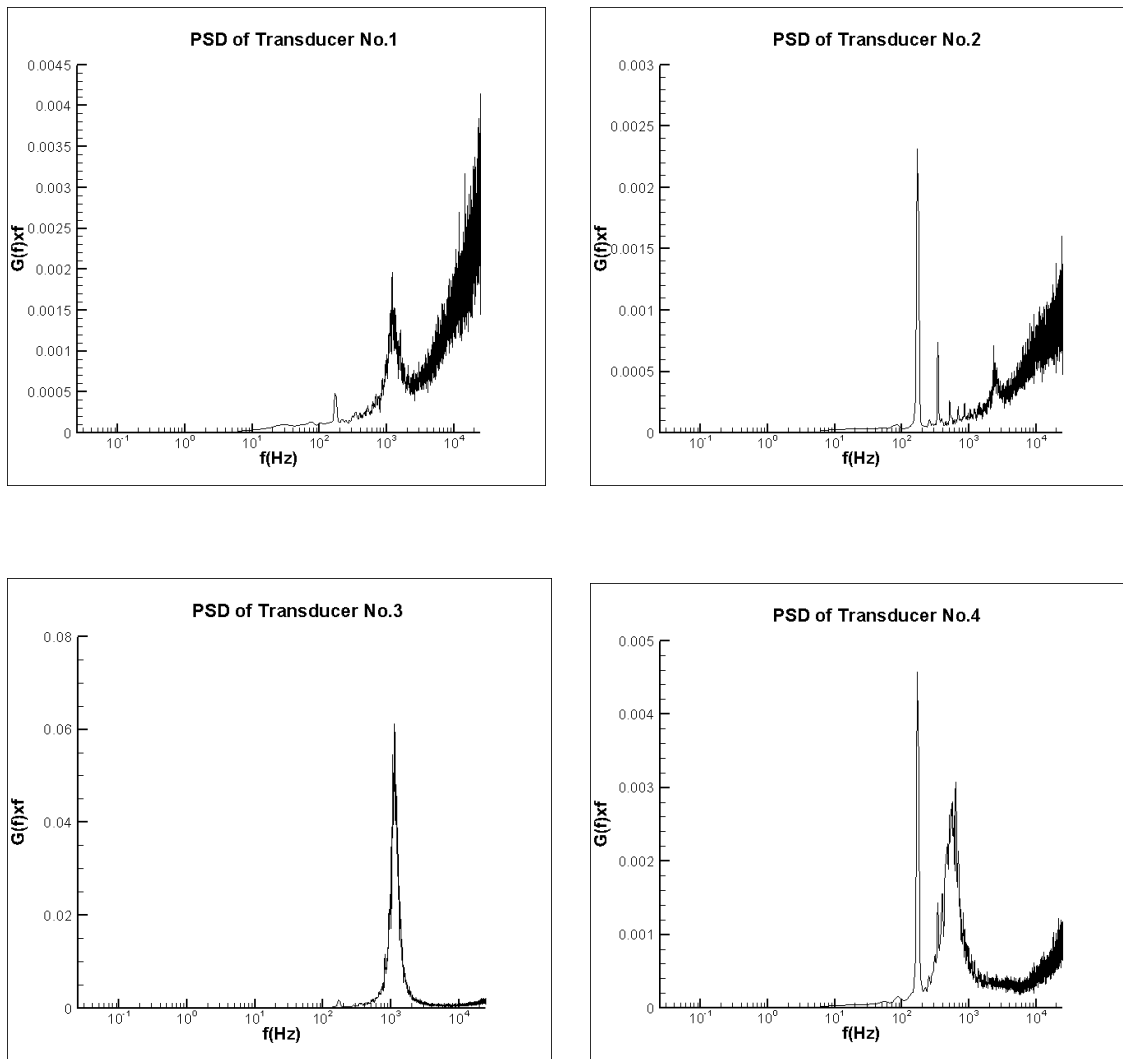


Figure 28. Power Spectral Density for 12° ramp (Corner flow) at Mach 3.3

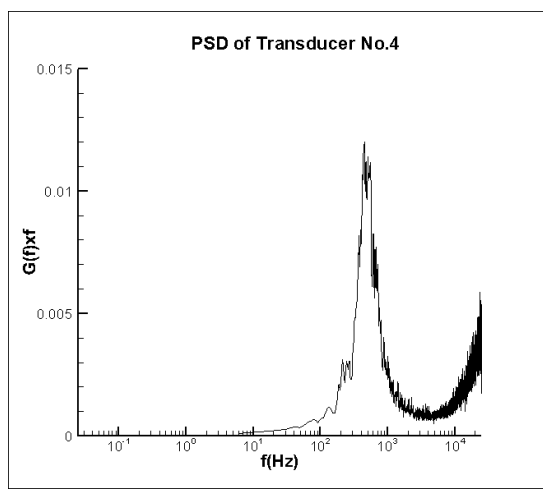
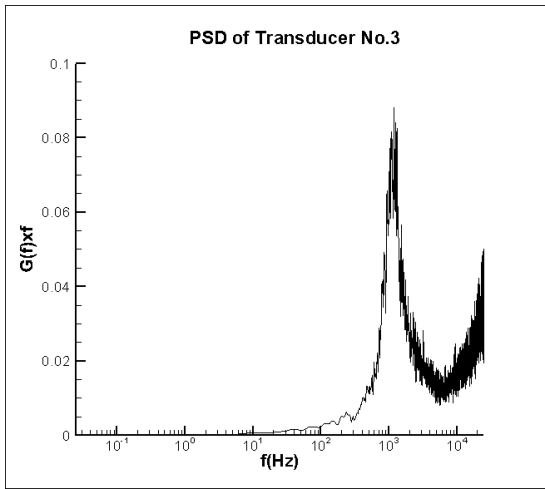
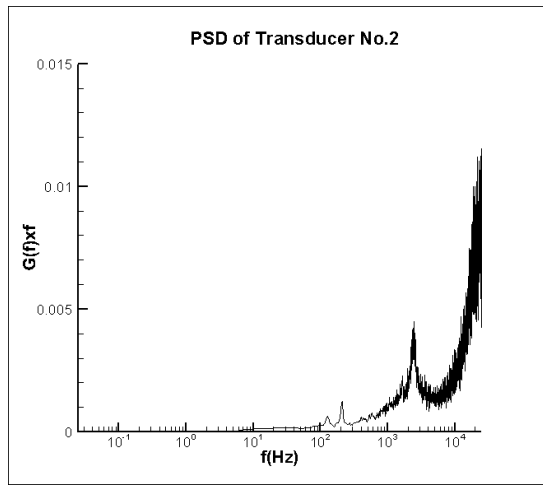
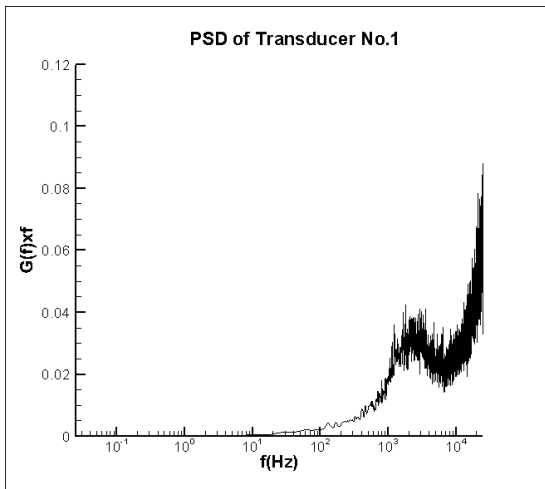


Figure 29. Power Spectral Density for 16° ramp (Corner flow) at Mach 2.5

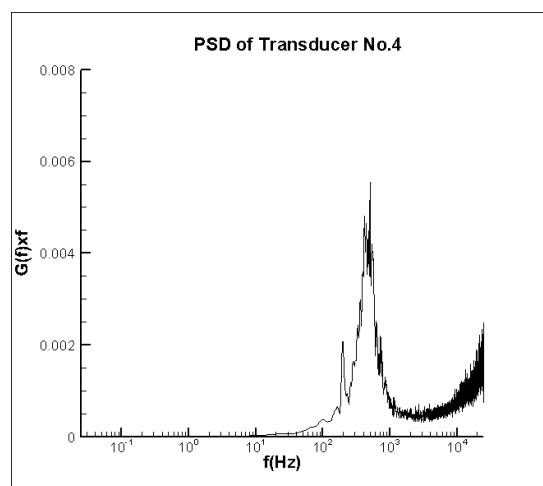
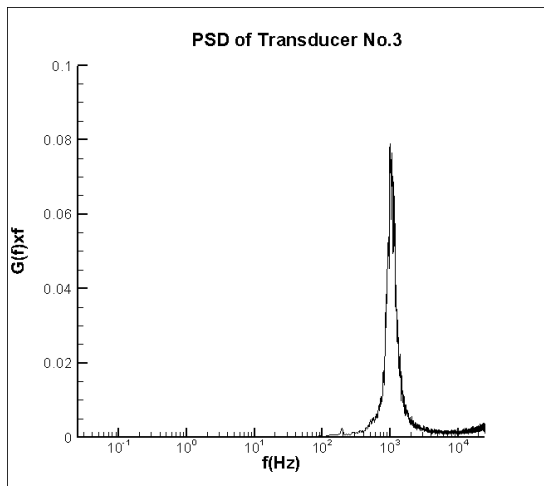
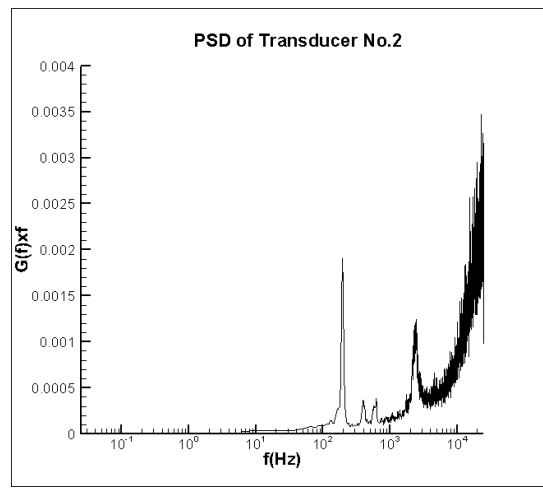
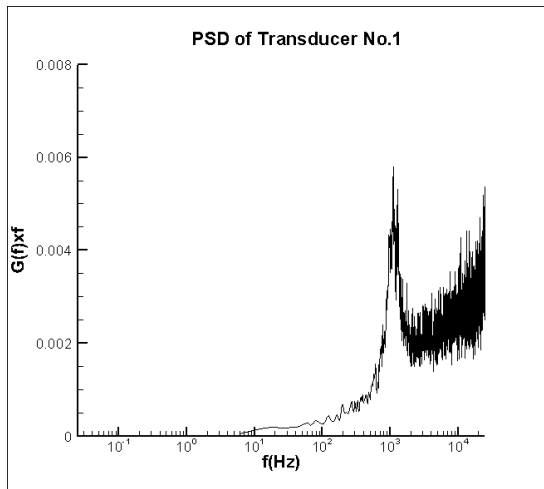


Figure 30. Power Spectral Density for 16° ramp (Corner flow) at Mach 3.3

The Power Spectral Density (PSD) is plotted for different configurations and Mach numbers in Figure 23, Figure 24, Figure 25, Figure 26, Figure 27, Figure 28, Figure 29, and Figure 30. The presence of shock unsteadiness is characterized by low frequencies (approx. 10^3 Hz). This is successfully captured by different transducers depending on the configuration and Mach number. Again, for centerline flow, if we compare the signature of shock unsteadiness for both the angles at the same Mach No., we observe that for the lower angled ramp, the transducer closer to the ramp edge has a PSD dominated by lower frequency indicating shock's lower proximity to the ramp with smaller angle. This also supports the conclusion drawn from the flow visualization.

CHAPTER-7 SUMMARY AND FUTURE WORK

This study examined the corner separation in an SBLI caused by an oblique shock wave. A flat plate fitted with two fences perpendicular to it acted as the rectangular channel that housed the corner SBLI. A compression ramp installed near the trailing edge of the plate generated the required oblique shock wave and simulated the SBLI along the centreline and at the corner. Prior to conducting the experiments, the characterization of the turbulent boundary developing on a flat plate was conducted. The characterization and the actual set of experiments were done at two test Mach numbers of 2.5 and 3.3.

The interaction was characterized qualitatively through schlieren imaging and surface oil flow visualization. Schlieren imaging provided a view of the shocks associated with the set up and confirmed the generation of the expected interaction. Surface oil flow visualization provided an observation of the growth of the corner boundary layer and flow separation. The flow separated and the interaction was three dimensional as observed from the corner vortices.

The interaction was characterized quantitatively by unsteady pressure measurements along the flow centreline and the corner. The pressure trends showed the smearing of the adverse pressure gradients due to corner separation at the lower Mach number and an unseparated corner boundary layer at the higher Mach number which is in good agreement with the observations made by Burton et al.(2010) and Bruce et al (2011).

A thorough iteration helped in arriving at the design of the present experimental set up that was successful in generating the corner SBLI which was free of any undulations. It provides a sound environment to conduct experiments on corner SBLI in future. Further, it is easy to

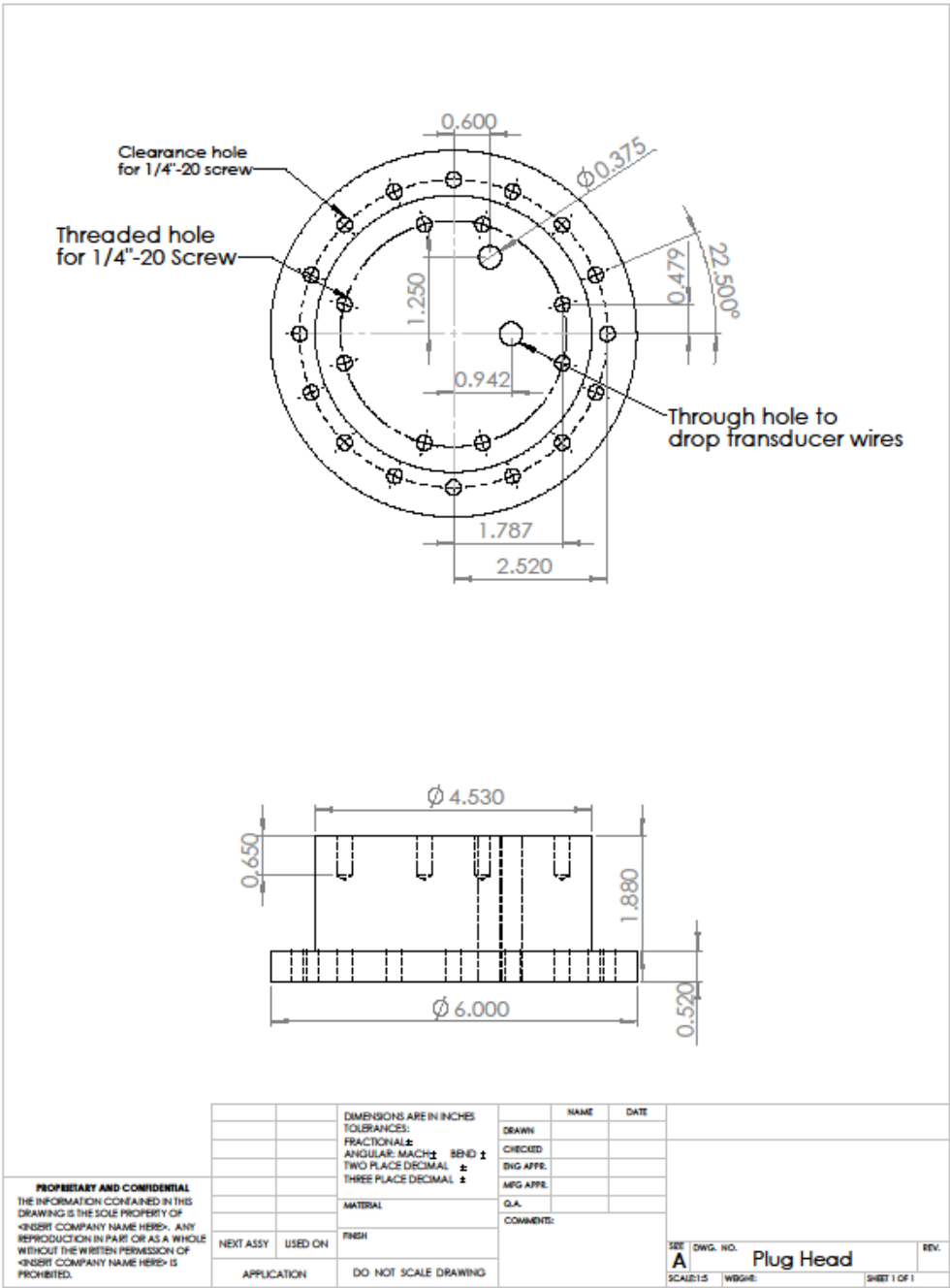
replicate/modify as per need, as the assembly is simple, involving few components. Further pursuit of research of this interaction may provide information regarding the dynamics of the SBLI to the flow control community.

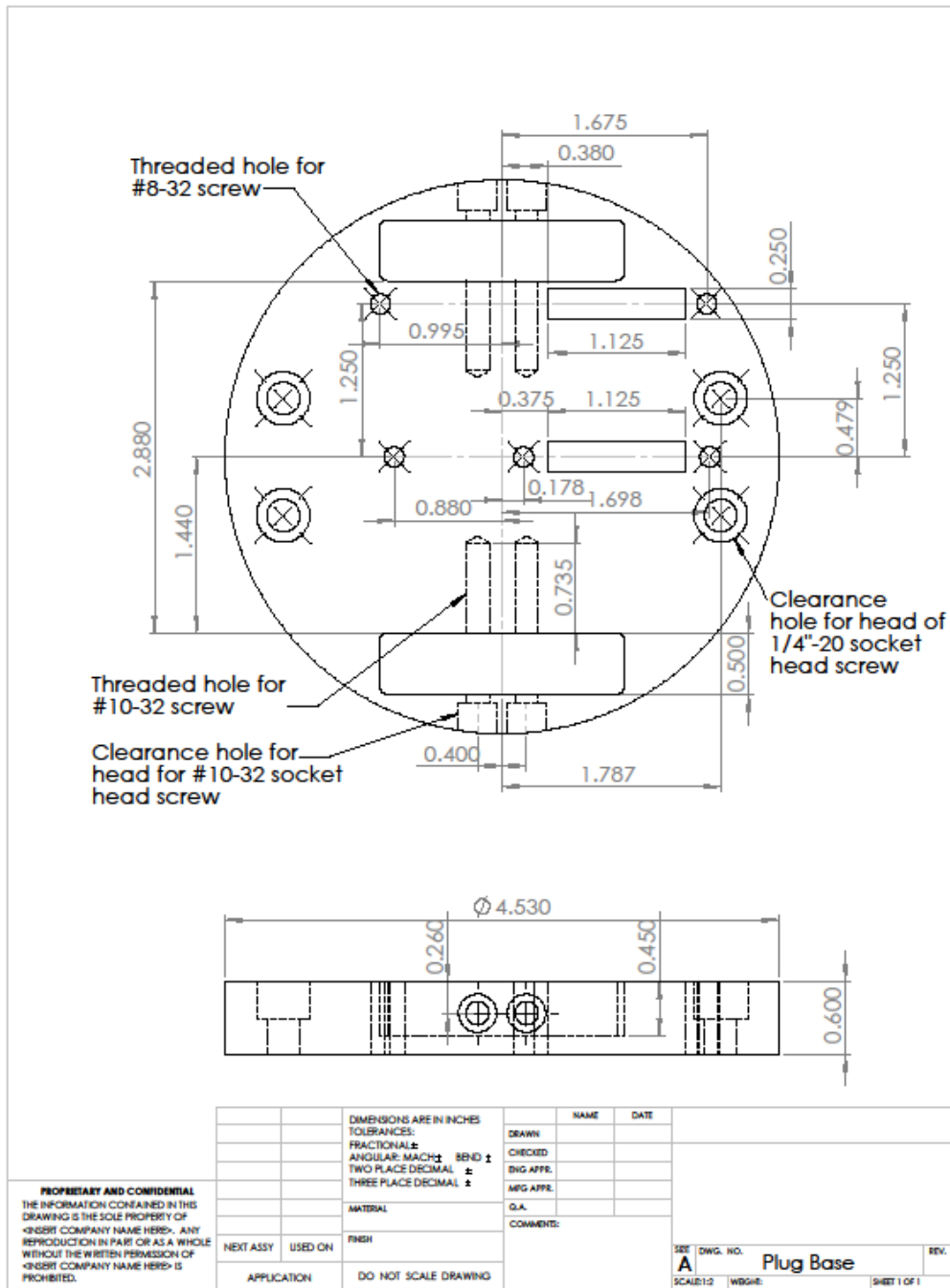
REFERENCES

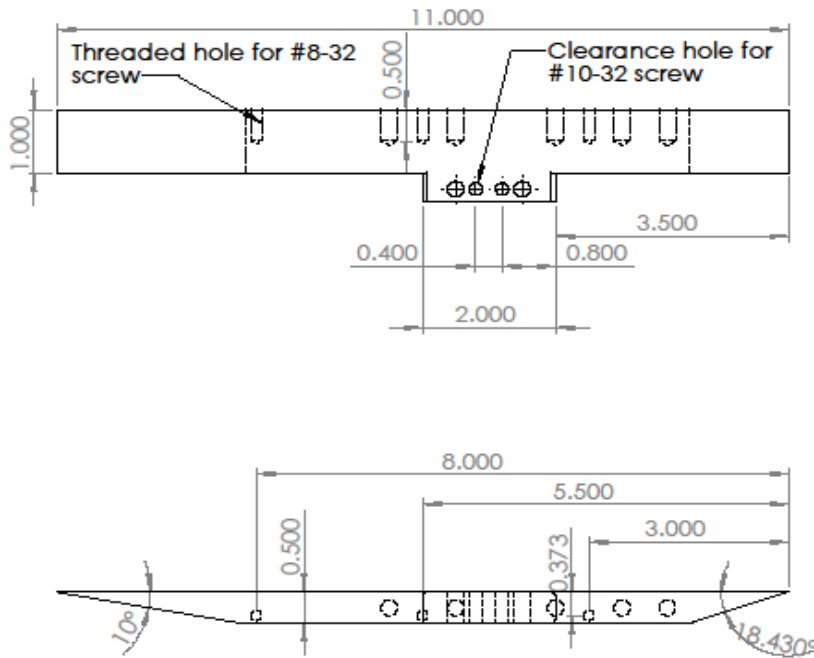
1. Venkateswaran Narayanaswamy, Laxminarayan L.Raja and Noel T.Clemens. Control of Unsteadiness of a shock wave/turbulent boundary layer interaction by using a Pulsed-Plasma jet actuator, *Physics of Fluids* 24,076101(2012)
2. D.M.F.Burton, H.Babinsky and P.J.K.Bruce. Experimental Investigation into Parameters Governing Corner Interactions for Transonic Shock Wave/Boundary layer Interactions, 48th AIAA Aerospace Sciences Meeting including the New Horizons Forum and Aerospace Exposition 04-07 January 2010, Orlando, Florida
3. A.N.Smith, H.Babinsky, J.L.Fulker and P.R.Ashill. Shock Wave/Boundary layer Interaction Control Using Streamwise Slots in Transonic Flows, *Journal of Aircraft* Vol.41, No.3, May-June 2004
4. Neil Titchener, Holger Babinsky and Eric Loth. Can Fundamental Shock-Wave/Boundary Layer Interaction Research be relevant to inlet Aerodynamics? 50th AIAA Aerospace Sciences Meeting including the New Horizons Forum and Aerospace Exposition 09-12 January 2012, Nashville, Tennessee
5. Aaron W.Porter. A Thesis on 'Characterization of a Supersonic Wind Tunnel for the study of Supersonic Inlet Flow Control', *The Ohio State University*, 2012.
6. D.M.F.Burton and H.Babinsky. Corner Separation Effects for normal shock wave/turbulent boundary layer interactions in rectangular channels, *J.Fluid Mech.*(2012), vol.707, pp 287-306
7. P.J.K. Bruce, D.M.F.Burton, N.A.Titchener and H.Babinsky. Corner effect and separation in transonic channel flows, *J.Fluid Mech.*(2011), vol.679, pp 247-262
8. Noel T.Clemens, Venkateswaran Narayanaswamy. Low Frequency Unsteadiness in Shock Wave/Turbulent Boundary Layer Interactions, *Annual Review of Journal of Fluid Mechanics* 2014 46:469-92

9. P.R.Viswanath.Shock wave-turbulent-boundary-layer interactions and its control: A survey of recent developments, *Sadhana Vol.12 Parts 1 & 2, February 1988, pp 45-104*
10. Michael Rybalko, H.Babinsky and Eric Loth. Vortex generators for a Normal Shock/Boundary Layer Interaction with a Downstream Diffuser, *Journal of Propulsion and Power, Vol. 28, No. 1, January-February 2012*
11. H.Babinsky, Y. Li and C.W.Pitt Ford. Microramp control of Supersonic Oblique/ Shock-wave/Boundary-Layer Interactions, *AIAA Journal Vol. 47, No.3, March 2009*
12. Eric Loth, Neil Titchener, Holger Babinsky and Louis Povinelli, Canonical Normal Shock Wave/Boundary-Layer Interaction Flows Relevant to External Compression Inlets, *AIAA Journal Vol. 51, No. 9, September 2013*
13. Andrew G.Dann and Richard G.Morgan. Analytical Method of Prediction of Turbulent Boundary-Layer Separation in Hypersonic Flows, *AIAA Journal Vol. 49, No. 9, September 2011*
14. Neil Titchener and Holger Babinsky. Shock Wave/Boundary-Layer Interaction Control Using a Combination of Vortex Generators and Bleed, *AIAA Journal Vol. 51, No. 5, May 2013*
15. R.L. Davis and J.E.Carter. Counter Rotating Streamline Pattern in a Transitional Separation Bubble, *AIAA Journal Vol. 25, No.5, May 1986*
16. Taro Handa Mitsuharu Masuda. Three-dimensional normal shock-wave/boundary-layer interaction in a rectangular duct, *AIAA Journal Vol. 43, No.10, October 2005*
17. M.E.Erengil and D.S.Dolling. Correlation of Separation Shock Motions with pressure fluctuations in the Incoming Boundary Layer, *AIAA Journal Vol. 29 No. 11, November 1991.*
18. D.O.Davis, F.B.Gessner and G.D. Kerlick. Supersonic Laminar Flow Development in a Square Duct, *AIAA Journal Vol. 25 No. 1, January 1987.*

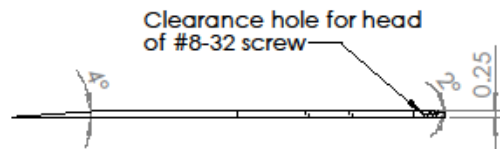
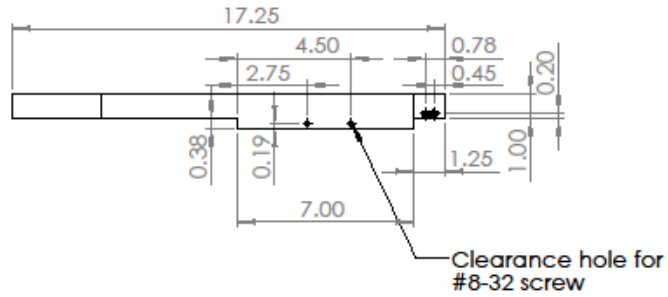
APPENDIX



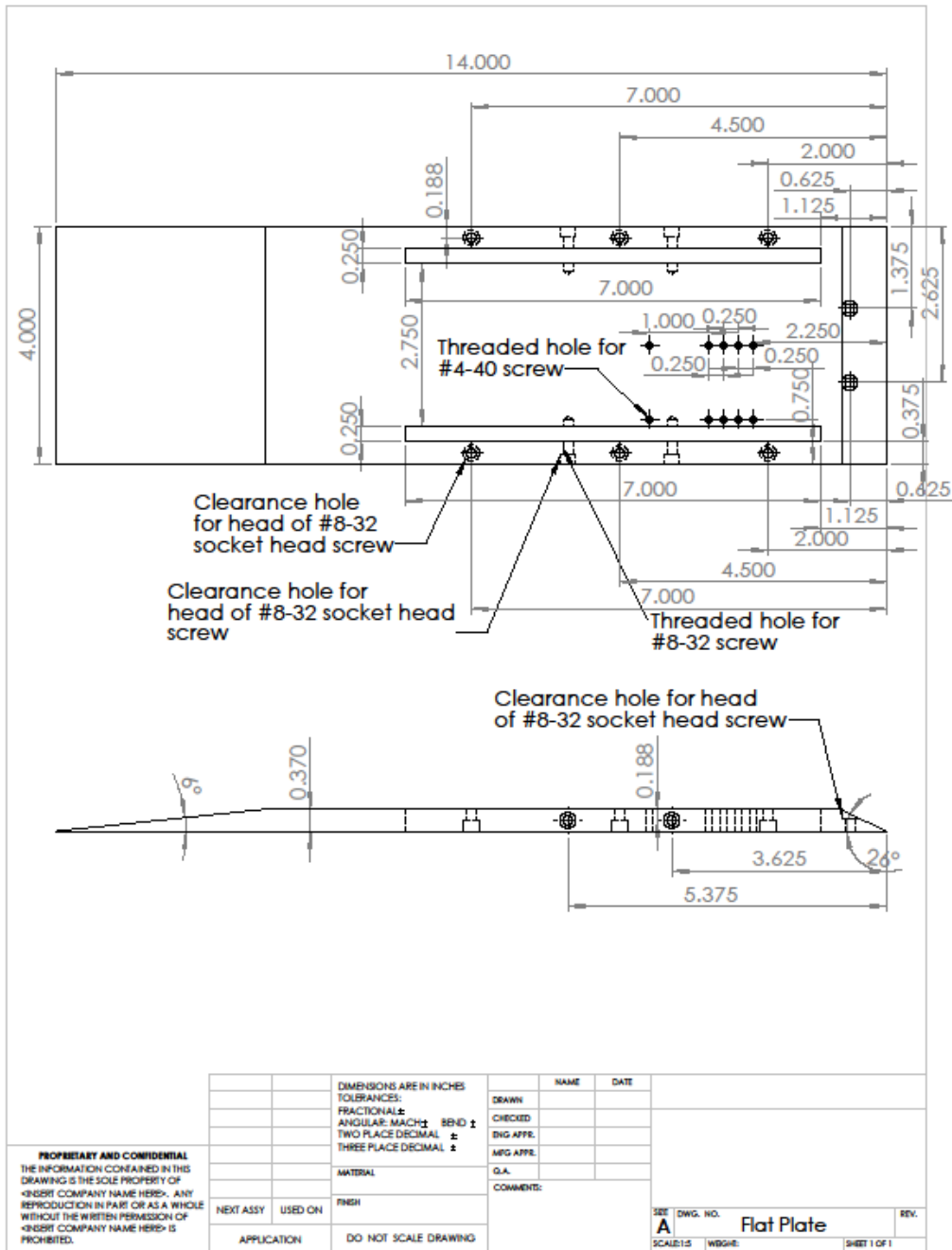




<p>PROPRIETARY AND CONFIDENTIAL THE INFORMATION CONTAINED IN THIS DRAWING IS THE SOLE PROPERTY OF <NSBT COMPANY NAME HERE>. ANY REPRODUCTION IN PART OR AS A WHOLE WITHOUT THE WRITTEN PERMISSION OF <NSBT COMPANY NAME HERE> IS PROHIBITED.</p>		DIMENSIONS ARE IN INCHES TOLERANCES: FRACTIONAL ± ANGULAR MATCH ± BEND ± TWO PLACE DECIMAL ± THREE PLACE DECIMAL ±		NAME	DATE
		DRAWN CHECKED ENG APPE. MFG APPE. Q.A. COMMENTS:			
NEXT ASSY	USED ON	MATERIAL	FINISH	SEE DWG. NO. A Mounting strut SCALE: 1:1 W89H: SHEET 1 OF 1	
APPLICATION	DO NOT SCALE DRAWING				



<p>PROPRIETARY AND CONFIDENTIAL THE INFORMATION CONTAINED IN THIS DRAWING IS THE SOLE PROPERTY OF <INSERT COMPANY NAME HERE>. ANY REPRODUCTION IN PART OR AS A WHOLE WITHOUT THE WRITTEN PERMISSION OF <INSERT COMPANY NAME HERE> IS PROHIBITED.</p>		DIMENSIONS ARE IN INCHES TOLERANCES: FRACTIONAL: ± ANGULAR: MACH: ± BEND: ± TWO PLACE DECIMAL: ± THREE PLACE DECIMAL: ±		NAME DATE	
		DRAWN CHECKED ENG APPE. MFG APPE. Q.A. COMMENTS:			
		MATERIAL			
NEXT ASSY	USED ON	FINISH			
APPLICATION		DO NOT SCALE DRAWING			
			SET DWG. NO. A SCALE: 1:5 WBBG#:	Fence SHEET 1 OF 1	REV.

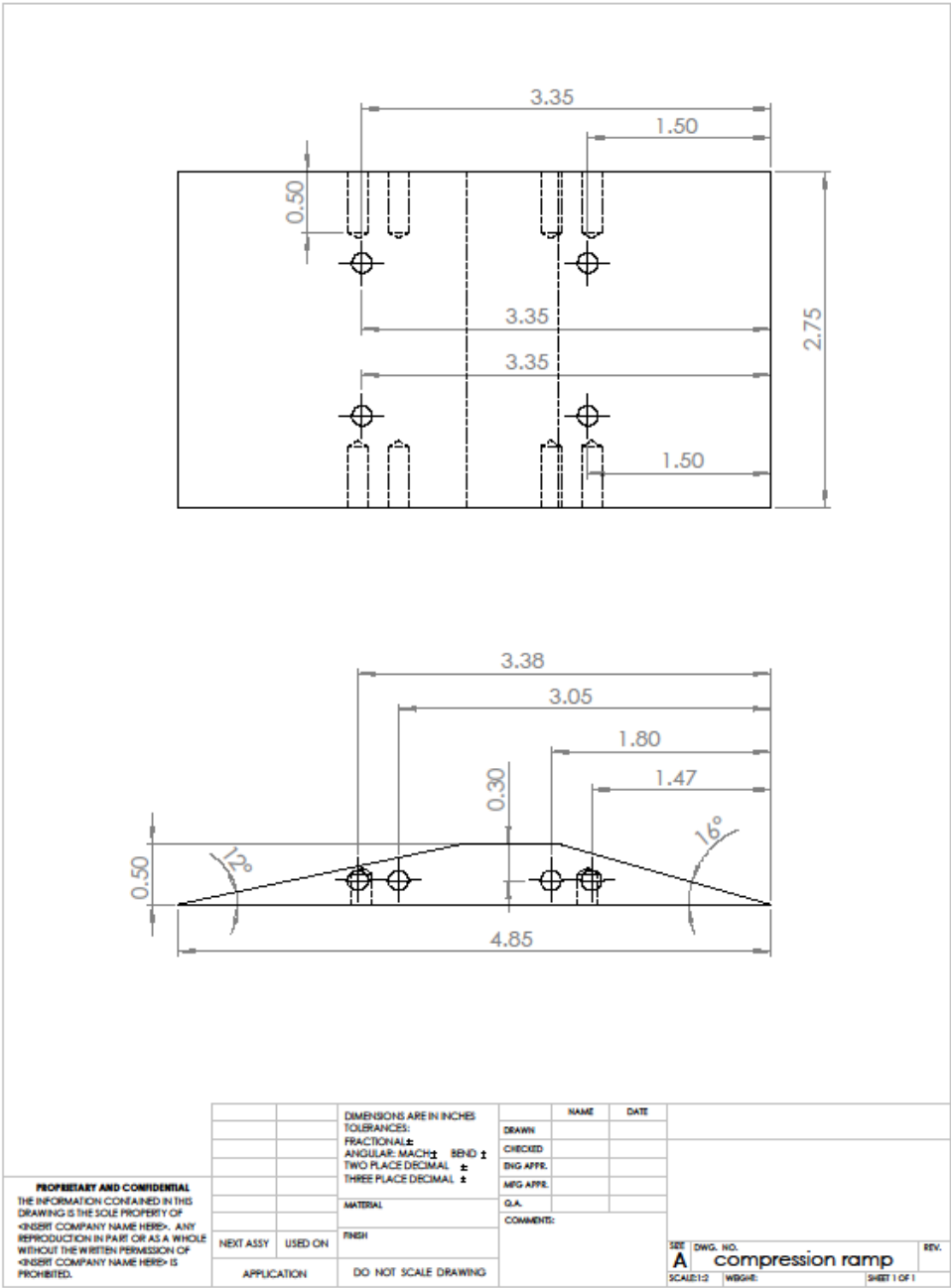


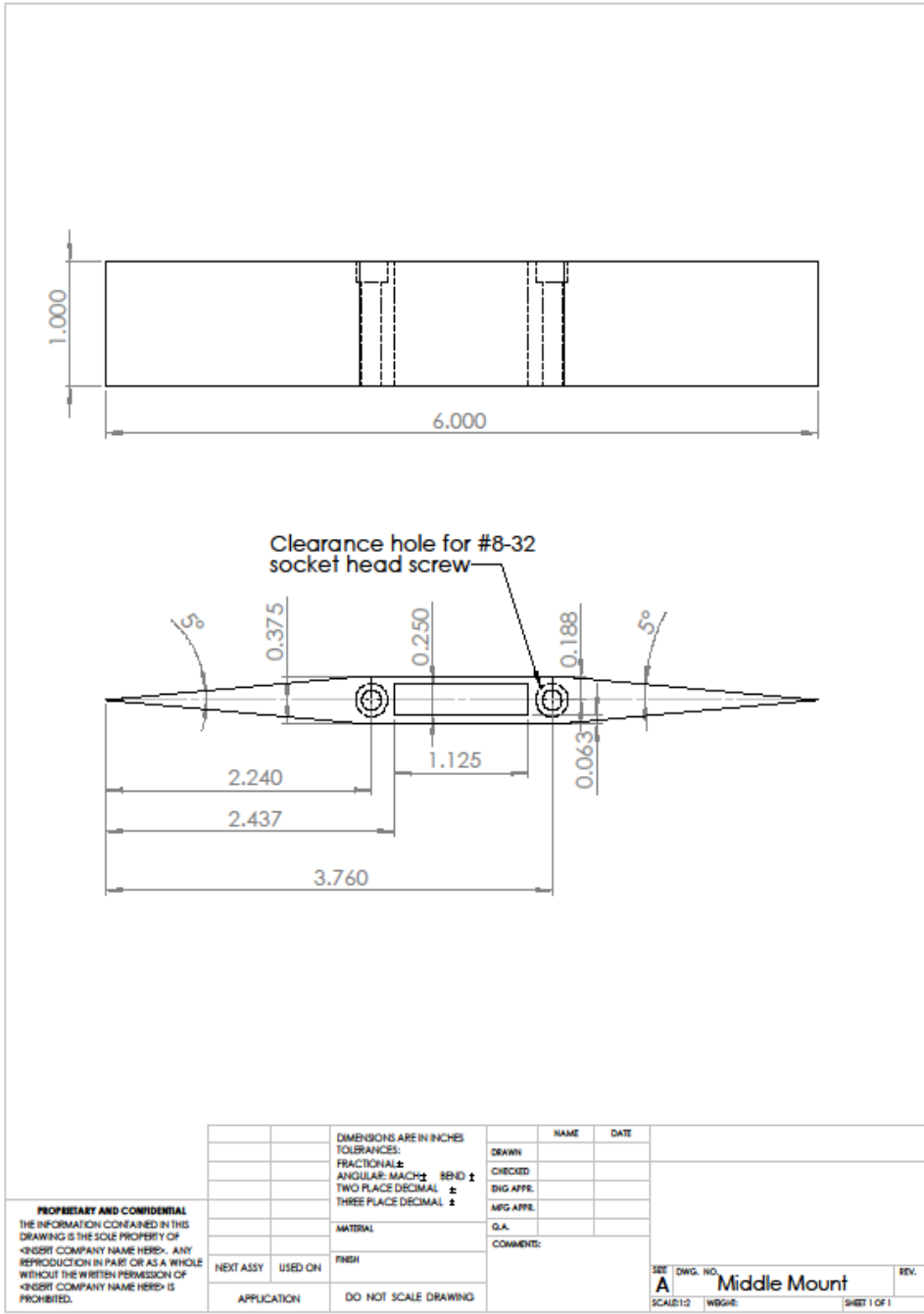
PROPRIETARY AND CONFIDENTIAL
 THE INFORMATION CONTAINED IN THIS DRAWING IS THE SOLE PROPERTY OF <INSERT COMPANY NAME HERE>. ANY REPRODUCTION IN PART OR AS A WHOLE WITHOUT THE WRITTEN PERMISSION OF <INSERT COMPANY NAME HERE> IS PROHIBITED.

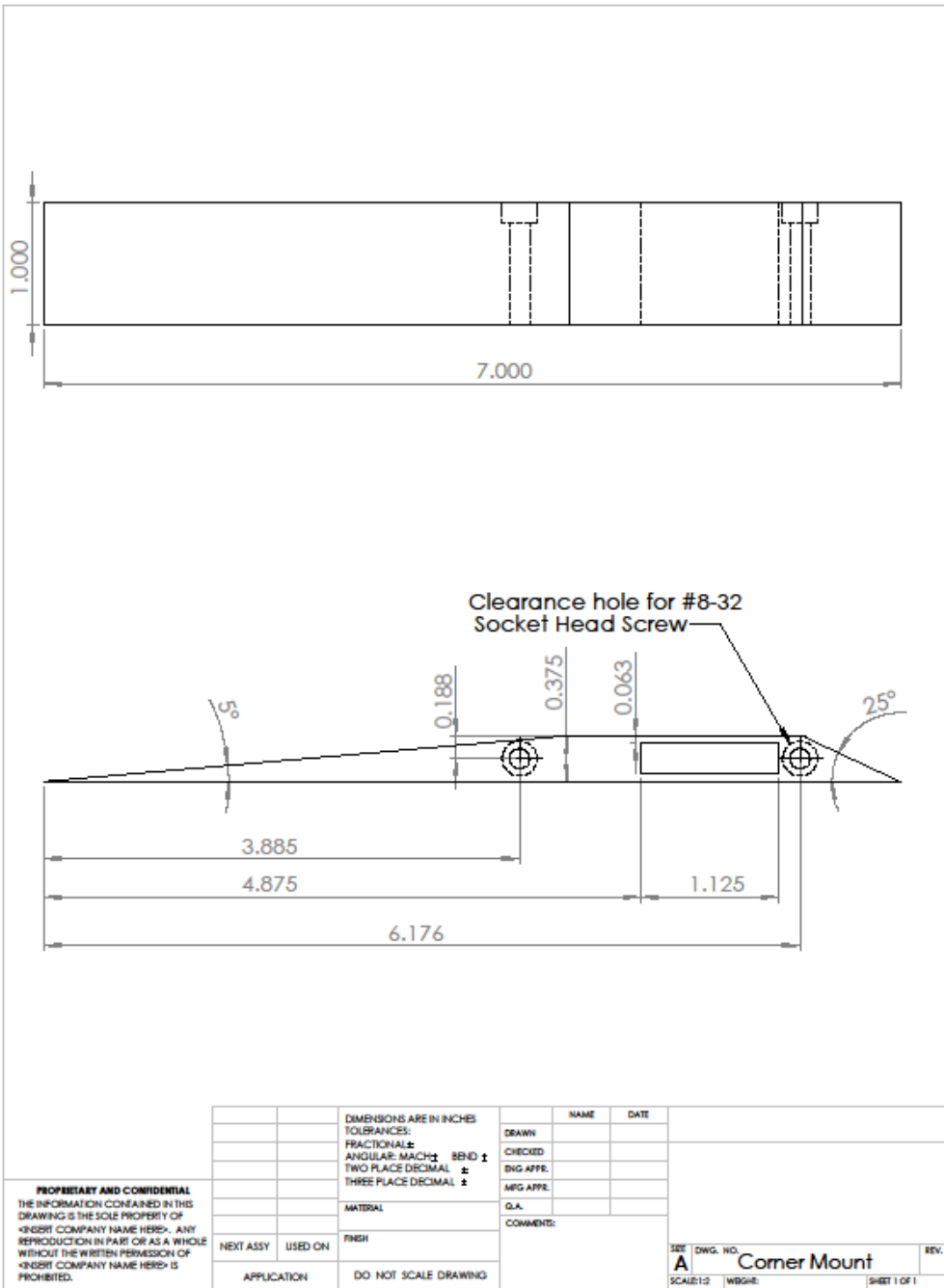
		DIMENSIONS ARE IN INCHES TOLERANCES: FRACTIONAL: ± ANGULAR: MACH ± BEND ± TWO PLACE DECIMAL ± THREE PLACE DECIMAL ±		
		MATERIAL		
		FINISH		
		APPLICATION		DO NOT SCALE DRAWING

	NAME	DATE
	DRAWN	
	CHECKED	
	ENG APPR.	
	MFG APPR.	
	Q.A.	
	COMMENTS:	

SEE	DWG. NO.	REV.
A	Flat Plate	
SCALE: 1:5	WG#:	SHEET 1 OF 1







PROPRIETARY AND CONFIDENTIAL
 THE INFORMATION CONTAINED IN THIS
 DRAWING IS THE SOLE PROPERTY OF
 <INSERT COMPANY NAME HERE>. ANY
 REPRODUCTION IN PART OR AS A WHOLE
 WITHOUT THE WRITTEN PERMISSION OF
 <INSERT COMPANY NAME HERE> IS
 PROHIBITED.

		DIMENSIONS ARE IN INCHES	NAME	DATE
		TOLERANCES:	DRAWN	
		FRACTIONAL: ±	CHECKED	
		ANGULAR: MACH ± BEND ±	ENG APPR.	
		TWO PLACE DECIMAL ±	MFG APPR.	
		THREE PLACE DECIMAL ±		
		MATERIAL	Q.A.	
NEXT ASSY	USED ON	FINISH	COMMENTS:	
APPLICATION		DO NOT SCALE DRAWING		

REV.	DWG. NO.	REV.
A	Corner Mount	
SCALE: 1:2	WGGE:	SHEET 1 OF 1